



1 **Nocturnal production of N₂O₅ and ClNO₂ in Delhi: driving factors and impacts**

2 Yijing Chen^{1,2}, Cheng Wu^{2*}, Epameinondas Tsiligiannis², Ravi Kant Pathak^{2,3}, Jan B. C. Pettersson²,
3 Harsh Raj Mishra^{2,3†}, Gazala Habib⁴, Geetam Tiwari⁵, Kebin He¹, Jingkun Jiang^{1*}, Mattias
4 Hallquist^{2*}

5 **Affiliations:**

6 ¹State Key Laboratory of Regional Environment and Sustainability, School of Environment, Tsinghua
7 University, School of Environment, Tsinghua University; Beijing, 100084, China.

8 ²Department of Chemistry and Molecular Biology, University of Gothenburg; Gothenburg, 40530,
9 Sweden.

10 ³Indo-Gangetic Plains Centre for Air Research and Education (IGP-CARE), Hamirpur, Uttar Pradesh,
11 210301, India.

12 ⁴Transportation Research and Injury Prevention Centre, Indian Institute of Technology Delhi, New
13 Delhi, 110016, India.

14 ⁵Department of Civil Engineering, Indian Institute of Technology Delhi, New Delhi, 110016, India.

15 [†]Present address: School of Earth and Atmospheric Sciences, Queensland University of Technology,
16 Queensland, 4001, Brisbane, Australia.

17

18 ***Correspondence to:** Mattias Hallquist (hallq@chem.gu.se), Jingkun Jiang (jiangjk@tsinghua.edu.cn)
19 and Cheng Wu (cheng.wu@gu.se).

20

21 **This PDF file includes:**

22 Abstract

23 Main Text

24 Figures 1 to 6

25

26

27

28

29



30 **ABSTRACT.**

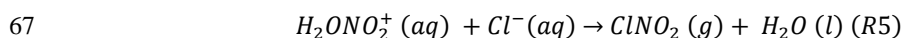
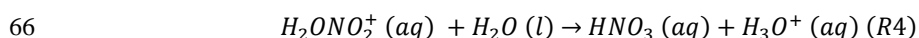
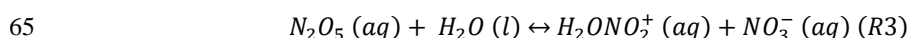
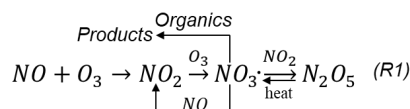
31 Nitryl chloride (ClNO_2) is an important $\text{Cl}\cdot$ precursor, originating from the heterogeneous reactions of
32 dinitrogen pentoxide (N_2O_5) on chloride-containing particles. This $\text{N}_2\text{O}_5\text{-ClNO}_2$ chemical process
33 plays critical roles in chloride activation, nitrate formation, and thus air pollution. Here we present
34 field measurements made in the early springtime of 2023 in Delhi and compare with a previous study
35 conducted during the winter of 2019. We found elevated nocturnal levels of N_2O_5 and ClNO_2 ,
36 averaging 13 and 80 ppt, respectively, which are approximately doubled compared to observations in
37 2019. This change is primarily driven by the reduced nighttime NO levels, from 124 ± 25 ppb in 2019
38 to 44 ± 9 ppb in 2023. In addition, the chloride concentration (nighttime average $4.7 \mu\text{g}/\text{m}^3$) in Delhi
39 is among the highest reported globally, driving efficient conversion of N_2O_5 to ClNO_2 . Decreased NO
40 and elevated ClNO_2 levels lead to higher $\text{NO}_3\cdot$ and $\text{Cl}\cdot$ production that promote the oxidation of
41 organics. Consistently, we observed increased fractions of gaseous nitrogen- and chlorine-containing
42 organic products and a higher oxidation state of the organic aerosols. Our findings highlight the need
43 for increased attention to atmospheric secondary pollution and stringent chlorine emissions control
44 with the reduction of NO_x in Delhi.

45



46 **1 INTRODUCTION**

47 Atmospheric N_2O_5 - ClNO_2 chemistry refers to the conversion of N_2O_5 to ClNO_2 on chloride-
48 containing particles (Finlayson-Pitts et al., 1989), which is ubiquitous worldwide (Wang et al., 2019)
49 and exerts profound impacts on nitrogen budgets (Dentener and Crutzen, 1993), chloride
50 activation (Thornton et al., 2010), and atmospheric oxidative capacity (Simpson et al., 2015; Yang et al.,
51 2022). N_2O_5 is formed from the reaction between $\text{NO}_3\cdot$ and NO_2 (R1), and the heterogeneous reactions
52 of N_2O_5 on atmospheric particles produce particulate nitrate and gaseous ClNO_2 (R2-R5) (Bertram and
53 Thornton, 2009). ClNO_2 is rather inert at night and undergoes negligible losses, while it photolyses to
54 produce $\text{Cl}\cdot$ during the daytime (Osthoff et al., 2008). Given the fast photolysis of $\text{NO}_3\cdot$ and thermal
55 decomposition of N_2O_5 , the N_2O_5 to ClNO_2 conversion is expected to happen mainly at night (Brown
56 and Stutz, 2012). The occurrence of this nocturnal chemistry was confirmed by direct field
57 observations of N_2O_5 and ClNO_2 in the urban coastal air (Osthoff et al., 2008; Riedel et al., 2012), and
58 later extended to polluted inland areas (Thornton et al., 2010; Phillips et al., 2012; Le Breton et al.,
59 2018a; Ma et al., 2023; Chen et al., 2023), where abundant NO_x and particulate chloride precursors co-
60 exist, with measured nighttime peak mixing ratios consistently up to several parts per billion by volume
61 (ppb), which are about an order of magnitude higher than those observed in the remote arctic and
62 marine regions (McNamara et al., 2019; Eger et al., 2019; Kercher et al., 2009).



68 However, in Delhi, one of the world's most polluted megacities, despite the abundance of
69 ingredients (i.e., particulate chloride and NO_x , **Fig. S1**) for N_2O_5 and ClNO_2 production, the measured
70 nighttime N_2O_5 and ClNO_2 levels are rather low during a wintertime campaign conducted in 2019
71 (Haslett et al., 2023). This is attributed to the fast reaction rate constant between NO and $\text{NO}_3\cdot$ ($k_{\text{NO+NO}_3\cdot}$,
72 $2.6 \times 10^{-11} \text{ cm}^3 \text{ molec}^{-1} \text{ s}^{-1}$ at 298 K) (Burkholder et al., 2020) and the extremely high NO concentrations
73 (several hundreds of ppb) in Delhi, which largely quenched nocturnal $\text{NO}_3\cdot$ (the reaction scheme R1)
74 and limited subsequent N_2O_5 and ClNO_2 production (Haslett et al., 2023). Notably, the 2019 campaign
75 predominantly captured severe pollution episodes in Delhi, with nighttime average concentrations of
76 NO (124 ppb) and chloride (21 $\mu\text{g}/\text{m}^3$) far exceeding typical ranges (50~100 ppb and 5~10 $\mu\text{g}/\text{m}^3$,
77 respectively; **Fig. S2b, d**). The evolution of N_2O_5 - ClNO_2 chemistry outside of such extreme pollution



78 events under different NO regimes remains unclear due to limited field observations in Delhi.

79 In this work, we present a recent field measurement of N_2O_5 , ClNO_2 and other relevant inorganic
80 and organic species in both gas and particle-phases during the early springtime of 2023 in Delhi. This
81 timing captures a broader range of NO concentrations (below 0.1 to hundreds of ppb) and chemical
82 conditions, which overlaps with but extends beyond previous studies that primarily focused on the
83 most polluted winter months. We characterize the changes in N_2O_5 - ClNO_2 chemistry relative to the
84 previous observation in winter 2019(Haslett et al., 2023) and examine the underlying driving factors
85 and impacts. The field derived kinetic parameter, quantified as the product of N_2O_5 uptake coefficient
86 ($\gamma_{\text{N}_2\text{O}_5}$) and ClNO_2 yield (f_{ClNO_2}), is also estimated and compared to those reported from other
87 atmospheric environments. We find enhanced N_2O_5 production driven by decreased NO concentrations,
88 and the formation of ClNO_2 is dependent on the chloride level in Delhi. The product of $\gamma_{\text{N}_2\text{O}_5} \times f_{\text{ClNO}_2}$
89 (average ~ 0.2) is at the upper end of the values observed around the world, indicating efficient N_2O_5
90 conversion to ClNO_2 in Delhi. We further investigate the impacts of associated increases in $\text{NO}_3\cdot$ and
91 $\text{Cl}\cdot$ production rates on the atmospheric oxidation of organics, utilizing concurrent measurements of a
92 wide range of molecular-level organic oxidation products.

93 **2 METHODS**

94 **2.1 Field observation overview**

95 The field campaign was performed at the Indian Institute of Technology Delhi campus (IIT Delhi,
96 28.54°N, 77.19°E; ~ 230 m above the sea level) from 15 February to 14 March in 2023. The valid
97 dataset collected during the early spring period (2/23-3/14) was used for analysis in this study. IIT
98 Delhi is a representative continental urban site situated at the north-western of Indo-Gangetic Plain,
99 which is frequently affected by intense anthropogenic emissions from biomass and waste burning
100 activities, traffic exhaust, power plants, and industries(Kumar et al., 2022; Bryant et al., 2023; Kashyap
101 et al., 2019; Rai et al., 2020), and potential biogenic emissions from the surrounding vegetations (**Fig.**
102 **S4**). All the instruments were installed in an air-conditioned laboratory on the 8th floor, the roof level
103 of the building, at a sampling height of approximately 30 m above the ground. Details of the
104 measurement design are found in the supplementary information (Text. S1).

105 **FIGAERO-I-CIMS.** N_2O_5 , reactive chlorines, and oxygenated organics were identified as iodide
106 clusters ($\text{M}\cdot\text{I}^-$) by a Filter Inlet for Gases and AEROSols Iodide-Chemical Ionization-Time of Flight
107 Mass Spectrometer (FIGAERO-I-HR-ToF-CIMS, hereafter as CIMS)(Lopez-Hilfiker et al., 2014).
108 Basic principles and configurations were similar to those described in previous field studies(Le Breton
109 et al., 2018a;Le Breton et al., 2018b). Each CIMS operation cycle consisted of background (flushing
110 inlet with ultrahigh purity N_2) (~ 2 min), ambient gas (~ 16 min), a second background (~ 2 min), and
111 $\text{PM}_{2.5}$ desorption measurements (~ 50 min) (**Fig. S5**). The raw signals in counts per second (cps) were
112 normalized by the sum of the reagent ions ($\text{I}^- + \text{I}\cdot\text{H}_2\text{O}^-$) and multiplied by 10^6 . During the field



113 campaign, ~0.3 lpm perfluoropentanoic acid in N₂ was injected into the CIMS (identified as C₅HF₉O₂I⁻)
114 every 1~2 days for mass calibration. The sensitivities of acetic acid, which was generated from a
115 permeation source (permeation rate of 184.5 ng/min at 40°C), was measured periodically on 2/27, 2/28,
116 3/5, 3/10, 3/12, and 3/14 to track the instrument stability, which was 0.27 ± 0.05 cps/ppt with a
117 variation of 17.7%.

118 Calibrations of gaseous species were conducted after the campaign under RH conditions (IH₂O⁻
119 to I⁻ ratio 0.42 ± 0.02) similar to those observed during the field measurement in Delhi (IH₂O⁻ to I⁻
120 ratio 0.40 ± 0.08), with sensitivities of 7.5, 3.6, 0.013, 13.6, and 0.29 cps/ppt for N₂O₅, ClNO₂, HCl,
121 chloroacetic acid, and acetic acid, respectively. The sensitivity of acetic acid measured post-campaign
122 (0.29 cps/ppt) agreed well with the on-site calibration result (0.27 cps/ppt), and therefore no additional
123 scaling was applied for the on-site sensitivities of the detected species. Sensitivities for Cl₂ (3.4
124 cps/ppt), NCl₃ (3.1 cps/ppt), and NHCl₂ (0.05 cps/ppt) were determined from our previous study (Chen
125 et al., 2025b). The detection limits were determined as three times the standard deviation of the hourly
126 averaged background signals, which were 0.6 ppt for N₂O₅, 1.6 ppt for ClNO₂, 0.6 ppt for Cl₂, 22.6
127 ppt for NHCl₂, 0.3 ppt for NCl₃, 209.1 ppt for HCl, and 2.5 ppt for chloroacetic acid. For the remaining
128 detected gaseous compounds, the maximum value of the calibrated sensitivities (chloroacetic acid,
129 13.6 cps/ppt) was used to derive conservative concentration estimates. For particulate compounds, the
130 calibrated sensitivity of levoglucosan (2.2×10^5 ions/ng) was applied to obtain lower-limit estimates, as
131 the detection of levoglucosan has recently been demonstrated to proceed at the collision
132 limit(Aggarwal et al., 2025).

133 **EDXRF**. Energy Dispersive X-ray Fluorescence (EDXRF; SPECTRO-XEPOS, AMETEK Inc.) was
134 used to determine the concentrations of K and Cl in PM_{2.5} samples. ED-XRF is a sensitive and non-
135 destructive technique which requires negligible sample pre-treatment and has been widely used for
136 measuring elements in ambient particles(Ogrizek et al., 2022;Unga et al., 2025). A total of 83 PM_{2.5}
137 samples were collected at 3 lpm on PTFE filters (25 mm in diameter) via a PM_{2.5} cyclone every 12
138 hours from 2/22 to 2/28 and every 4 hours from 3/1 to 3/14. We increased the frequency of filter
139 switches by the end of the campaign to capture the variations of Cl element concentrations within a
140 night, i.e., before (19:00~23:00) and post (23:00~3:00) midnight. The mid-point of the measurement
141 period, i.e., 1:00 indicates measurement from 23:00~3:00, 5:00 for 3:00~7:00, 9:00 for 7:00~11:00,
142 13:00 for 11:00~15:00, 17:00 for 15:00~19:00, and 21:00 for 19:00~23:00, was used as the
143 representative timestamp for each filter sample.

144 The EDXRF instrument detects the total concentrations of elements in the collected filter samples,
145 while the CIMS detects compounds that evaporate at temperatures up to 200 °C. Persistent signals of
146 HCl·I⁻ were observed from PM_{2.5} desorption during the CIMS measurement (**Fig. S5**), likely
147 originating from the thermal decomposition of non-refractory chloride (e.g, NH₄Cl). The trend of
148 chloride measured by CIMS (pCl⁻-CIMS) largely followed that of the XRF-measured chloride (Cl-



149 XRF) ($r = 0.70$) (Fig. S6c). However, the campaign-averaged pCl-CIMS ($0.02 \mu\text{g}/\text{m}^3$) was
150 approximately two orders of magnitude lower than Cl-XRF ($2.3 \mu\text{g}/\text{m}^3$), likely due to the use of
151 levoglucosan sensitivity for quantification and negligible decomposition and desorption of alkali
152 chlorides (e.g., NaCl and KCl) in CIMS measurements. Nevertheless, pCl-CIMS was used
153 qualitatively to complement the temporal trend of Cl-XRF to hourly time-resolution.

154 Supporting measurements at IIT Delhi include trace gases (NO, NO₂, O₃, SO₂, and CO) and
155 meteorological parameters (T, RH, wind speed, and wind direction). Hourly PM_{2.5} concentrations and
156 solar radiation data were obtained from the nearest national monitoring station, the R.K. Puram station
157 operated by Delhi Pollution Control Committee (DPCC), which is located approximately 3 km
158 northwest of IIT Delhi. Intercomparison of the trace gases, T, and RH measured at IIT Delhi and R.K.
159 Puram showed overall good agreement (Fig. S6a); therefore, data from R.K. Puram were used to
160 supplement the analysis when measurements were not available at IIT Delhi. The aerosol surface area
161 (Sa) was estimated from the linear correlation between the measured Sa at IIT Delhi and PM_{2.5} in a
162 previous study (Gani et al., 2020) (Fig. S6b, $r = 0.78$). The solar radiation was converted to photolysis
163 frequency of J_{NO_2} utilizing the method from Trebs et al (Trebs et al., 2009). The estimated J_{NO_2} was
164 then used to derive real-time photolysis frequency of NO₃[·], O₃ and reactive chlorines (Chen et al.,
165 2025b). Additional details about the field observations are shown in Text S1.

166 Comparison with the measurements in 2019 (Haslett et al., 2023) was used to investigate the
167 evolution of N₂O₅-ClNO₂ chemistry under different chemical regimes in Delhi. It is noted that
168 throughout the manuscript, “in 2023” and “in 2019” refer to the corresponding field campaigns
169 conducted from 23 February to 14 March in 2023 (this study) and from 11 January to 5 February in
170 2019 (the previous campaign), respectively.

171 2.2 Kinetic calculations

172 **N₂O₅-ClNO₂ chemistry.** Key kinetic parameters were derived to investigate factors controlling the
173 variations of N₂O₅ and ClNO₂ and compare with previous studies. The field-constrained uptake
174 parameter, defined as the product ($\gamma_{N_2O_5} \times f_{ClNO_2}$) of the N₂O₅ uptake coefficient ($\gamma_{N_2O_5}$) and ClNO₂
175 yield (f_{ClNO_2}), as is shown in Eq. 1, was calculated hourly using neighboring measurements during the
176 nighttime following Eq. 3b in Mielke et al.(Mielke et al., 2013) (Eq. 1), assuming the local
177 heterogeneous uptake of N₂O₅ was the sole source of the measured ClNO₂ and that ClNO₂ experienced
178 negligible nocturnal losses.

$$179 \quad [\gamma_{N_2O_5} \times f_{ClNO_2}]_{t_0} = \frac{[ClNO_2]_{t_1}}{\int_{t_0}^{t_1} \frac{1}{4} \bar{c} S_a [N_2O_5]_{t_0} dt} \quad (\text{Eq. 1})$$

180 where \bar{c} is the average molecular velocity of N₂O₅ ($\sqrt{\frac{8kT}{\pi M_w}}$, k is Boltzmann's constant, 1.38×10^{-21}



181 $^{23} \text{ m}^2 \text{ kg}^{-1} \text{ s}^{-2} \text{ K}^{-1}$, T is temperature in Kelvin, Mw is the molecular weight of N_2O_5). The theoretical
182 values of the uptake parameter ($\gamma_{\text{N}_2\text{O}_5} \times f_{\text{ClNO}_2}$) range from 0 to 0.1, as the maximum values of $\gamma_{\text{N}_2\text{O}_5}$
183 and f_{ClNO_2} are generally below 0.1 and 1, respectively(Tham et al., 2018). However, nocturnal
184 transport, i.e., changes in air masses, can invalid this method and yield either negative (corresponding
185 to decreases in ClNO_2 , occurrence frequency of $\sim 38\%$) or unusually high values exceeding 0.1 (sharp
186 increases in ClNO_2 , occurrence frequency of $\sim 17\%$). The negative values were not considered for
187 further analysis and the extremely high values were discussed separately (**Section 3.2, Fig. 4**).

188 The production rate ($P(\text{NO}_3)$) and reactivity ($R(\text{NO}_3)$) of $\text{NO}_3\cdot$ were calculated to evaluate N_2O_5
189 budgets, which are shown in Eq. 2 and Eq. 3, respectively. The ClNO_2 production efficiency ($\varepsilon(\text{ClNO}_2)$,
190 Eq. 4), indicating the fraction of the total generated $\text{NO}_3\cdot$ overnight that is ultimately transformed into
191 ClNO_2 , was calculated for comparison with previous studies(Eger et al., 2019;Xia et al., 2025). The
192 integration period was set from 20:00 to 04:00 to minimize influences of potential air mass mixing
193 during the day-night and night-day transition periods.

194
$$P(\text{NO}_3) = k_{\text{NO}_2+\text{O}_3} [\text{NO}_2] [\text{O}_3] \quad (\text{Eq. 2})$$

195
$$R(\text{NO}_3) = k_{\text{NO}+\text{NO}_3} [\text{NO}] + J_{\text{NO}_3} + k_{\text{hete}} [\text{NO}_2] K_{eq} + \sum k_i [\text{VOC}_i] \quad (\text{Eq. 3})$$

196
$$\varepsilon(\text{ClNO}_2) = \frac{[\text{ClNO}_2]_{max}}{\int_{20:00}^{04:00} P(\text{NO}_3)} \quad (\text{Eq. 4})$$

197 where $k_{\text{NO}_2+\text{O}_3} = 1.2 \times 10^{-13} \times \exp(-2450/T) \text{ cm}^3/\text{molecule/s}$ and $k_{\text{NO}+\text{NO}_3} = 1.8 \times$
198 $10^{-11} \times \exp(110/T) \text{ cm}^3/\text{molecule/s}$ (Burkholder et al., 2020). J_{NO_3} is the photolysis frequency of
199 $\text{NO}_3\cdot$ and is retrieved from the Tropospheric Ultraviolet and Visible (TUV) radiation model and scaled
200 with the field constrained J_{NO_2} as discussed previously, k_{hete} is the first-order heterogenous loss
201 rate coefficient of N_2O_5 , which is calculated as $\frac{\bar{c}\gamma_{\text{N}_2\text{O}_5}}{4} S_a$. Here $\gamma_{\text{N}_2\text{O}_5}$ was parametrized as a function
202 ($\gamma_{\text{N}_2\text{O}_5} = RH \times 5.2 \times 10^{-4}$) of ambient RH up to 57% RH and then being a constant (0.03) according
203 to the experimental measurements of N_2O_5 uptake on aqueous organic aerosols(Evans and Jacob,
204 2005;Thornton et al., 2003). This parameterization method was supported by the consistency between
205 the simulated nocturnal ClNO_2 variations using the RH-parameterized $\gamma_{\text{N}_2\text{O}_5}$ and the observed ClNO_2
206 levels, as detailed in **Text S2**. K_{eq} is the equilibrium constant between $\text{NO}_3\cdot$, NO_2 , and N_2O_5 , where
207 $K_{eq} = 5.5 \times 10^{-27} \times \exp(10724/T)$ (Wängberg et al., 1997). $\sum k_i [\text{VOC}_i]$ is the sum of
208 $\text{NO}_3\cdot$ reactivity with different VOCs and we applied the same value of 0.081 s^{-1} in 2023 as in
209 2019(Haslett et al., 2023) due to the lack of concurrent VOCs measurements in 2023. This assumption
210 is not expected to significantly affect the estimated total $\text{NO}_3\cdot$ reactivity in 2023, which was still
211 dominated by the reactivity with NO (15.6 s^{-1} , **Fig. S7a**).

212 **Production rates of $\text{Cl}\cdot$ and $\text{OH}\cdot$ radicals.** The $\text{Cl}\cdot$ production rate ($P(\text{Cl}\cdot)$) is calculated according



213 to Eq. 5, where J is the photolysis frequency of each photolabile chlorines. For the 2023 campaign, we
214 calculated $P(Cl\cdot)$ both from $ClNO_2$ photolysis and from all the detected photolabile reactive chlorines.
215 A direct comparison between 2019 and 2023 was conducted using $P(Cl\cdot)$ from $ClNO_2$ photolysis. In
216 2019, only $ClNO_2$ photolysis was considered as a source of $Cl\cdot$, since mixing ratios of other
217 $Cl\cdot$ precursors were not reported in the previous study(Haslett et al., 2023). Additionally, we estimated
218 a lower-limit $OH\cdot$ production rate ($P(OH\cdot)$) in Delhi from the photolysis of O_3 in the presence of water
219 vapor (Eq. 6)(Dunlea and Ravishankara, 2004).

220
$$P(Cl) = J_{ClNO_2}[ClNO_2] + 2 \times J_{Cl_2}[Cl_2] + J_{NCl_3}[NCl_3] + J_{NHCl_2}[NHCl_2] \quad (Eq. 5)$$

221
$$P(OH) = \frac{2 \times J_{O^1D}[O_3] + k_{H_2O}[H_2O]}{k_{H_2O}[H_2O] + k_{N_2}[N_2] + k_{O_2}[O_2]} \quad (Eq. 6)$$

222 where J_{O^1D} is the photolysis frequency of O_3 , $k_{H_2O} = 1.6 \times 10^{-10} \times \exp(60/T)$, $k_{N_2} = 2.2 \times$
223 $10^{-11} \times \exp(110/T)$, and $k_{O_2} = 3.3 \times 10^{-11} \times \exp(55/T)$ (Burkholder et al., 2020).

224 **3 RESULTS AND DISCUSSION**

225 **3.1 Characteristics of N_2O_5 and $ClNO_2$ variations**

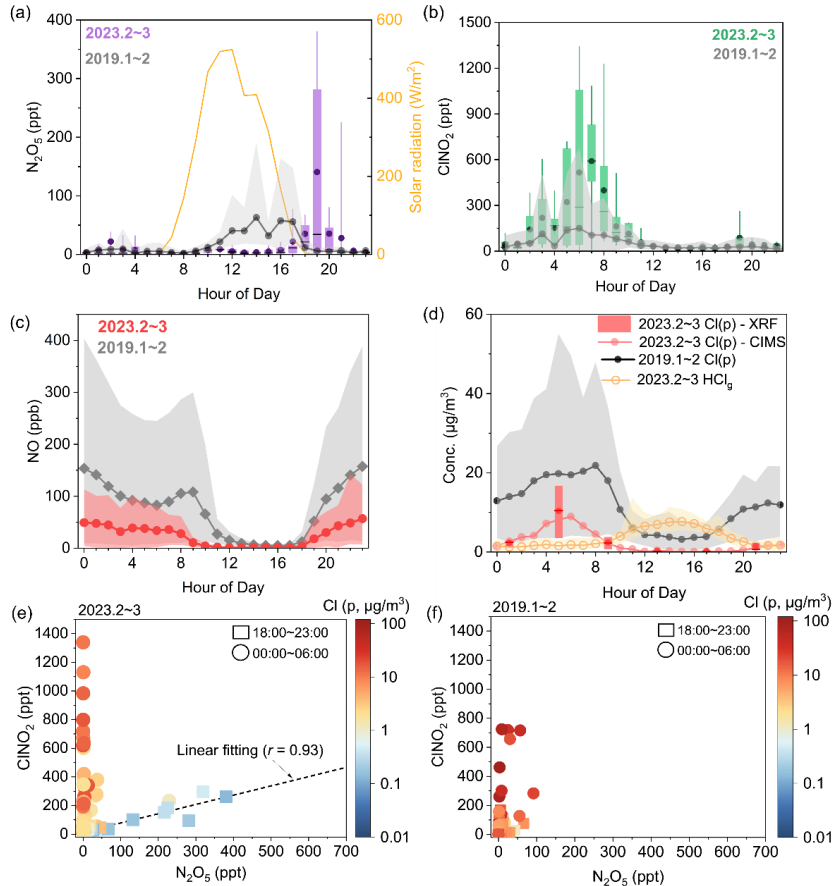
226 We observed frequent nocturnal enrichment of N_2O_5 and $ClNO_2$ in 2023 (**Figs. 1a-b**). Appreciable
227 N_2O_5 and $ClNO_2$ up to 566 and 1340 ppt were measured during the nighttime, with mixing ratios
228 commonly exceeding 10 and 100 ppt, respectively (**Fig. S8**). As shown in **Table S1**, the maximum
229 N_2O_5 mixing ratio in Delhi is a third to half of those observed in urban areas of the United
230 States(Thornton et al., 2010;Osthoff et al., 2008) and England(Bannan et al., 2015), and approximately
231 an order of magnitude lower than those measured in aged air plumes from industrial regions in
232 China(Chen et al., 2023;Wang et al., 2016;Ye et al., 2021). By contrast, the peak $ClNO_2$ levels in Delhi
233 are much higher than those reported in urban regions of the North America(Thornton et al.,
234 2010;McNamara et al., 2020;Wang et al., 2023a) and Europe(Bannan et al., 2015;Phillips et al.,
235 2012;Priestley et al., 2018), and similar to or 1~2 times lower than those observed in the North China
236 Plain(Tham et al., 2016b;Xia et al., 2021;Peng et al., 2021;Chen et al., 2025a), which implies efficient
237 conversion of N_2O_5 to $ClNO_2$ in Delhi.

238 The measured N_2O_5 generally presents transient, spike-like patterns in 2023 (**Fig. S8**), peaking
239 around the early evening (18:00~20:00) when both NO and particulate Cl are relatively low, and
240 tapering off as the night proceeds (**Figs. 1a, c-d**). In comparison, the $ClNO_2$ mixing ratio was gradually
241 built up after midnight with the increase of particulate Cl, reaching the highest level during the early
242 morning hours (06:00~08:00, **Figs. 1b, d**). Overall, the nocturnal N_2O_5 mixing ratio shows a significant
243 negative dependency ($r = -0.64$, $p < 0.01$) on the NO concentration (**Fig. 2a**), and $ClNO_2$ exhibits a
244 positive correlation with the particulate Cl level (**Fig. S9a**), indicating the critical roles of NO and
245 chloride in controlling N_2O_5 and $ClNO_2$ formation in Delhi.



246 We further examined N_2O_5 and ClNO_2 variations every night and classified them into the
247 enhanced and non-enhanced cases (**Figs. S10-S11**). Among the enhanced cases, elevated N_2O_5 mixing
248 ratios exceeding 10 ppt were characterized by both relatively low NO (median 3 ppb) and particulate
249 Cl (median $0.7 \mu\text{g}/\text{m}^3$) concentrations, and appreciable ClNO_2 levels larger than 100 ppt were observed
250 under moderate NO (median 7 ppb) and high particulate Cl (median $3.3 \mu\text{g}/\text{m}^3$) conditions (**Fig. S10**).
251 No notable N_2O_5 or ClNO_2 mixing ratios were measured among the non-enhanced cases when NO
252 levels were relatively high (median 31 ppb) (**Fig. S11**). The occurrence frequency of the enhanced
253 cases (11 out of total 19 nights) is higher than the non-enhanced (8 nights) cases.

254 The nocturnal abundances of N_2O_5 and ClNO_2 increase in 2023 compared to 2019. Overall, the
255 nighttime N_2O_5 and ClNO_2 mixing ratios in 2023, with an average of 13.1 ppt and 80.1 ppt, respectively,
256 are significantly (Mann-Whitney test, $p < 0.01$) higher than those measured in 2019 (4.5 and 36.3 ppt,
257 respectively) (**Figs. 1a-b**). The nocturnal mean ClNO_2 production efficiency ($\varepsilon(\text{ClNO}_2)$) also increases
258 from 3.0% in 2019 to 4.3% in 2023, which is comparable to the values reported in marine and coastal
259 areas (Eger et al., 2019; Xia et al., 2025). In addition, the diurnal profile of N_2O_5 in 2023 was inverted
260 compared to 2019, with higher levels in the early evening rather than during the daytime (**Fig. 1a**).
261 Consistently, distinct diurnal variations of N_2O_5 were also observed under relatively low- and high-
262 NO conditions in 2023 (**Fig. S12**). The emerging early evening peak of N_2O_5 leads to a new N_2O_5 -
263 driven ClNO_2 enhancement pattern in 2023, characterized by a strong positive correlation ($r = 0.93$)
264 between N_2O_5 and ClNO_2 under conditions of elevated N_2O_5 (10~400 ppt) and limited particulate Cl
265 concentrations ($0.1\text{--}3.4 \mu\text{g}/\text{m}^3$) (**Figs. 1e-f**). This pattern resembles those observed in other continental
266 air masses (Thornton et al., 2010; Bannan et al., 2015; Zhou et al., 2018), while the ClNO_2 to N_2O_5 ratios
267 are slightly higher in Delhi, ranging from 0.3 to 3.2, with an average of 1.2. Notably, despite the
268 substantial decline in particulate Cl from 2019 ($20.8 \mu\text{g}/\text{m}^3$) to 2023 ($4.7 \mu\text{g}/\text{m}^3$), the higher ClNO_2
269 levels in 2023 indicate that the promoting effect of elevated N_2O_5 potentially outcompetes the limiting
270 impact of reduced chloride. Additionally, chloride is likely still sufficient to maintain a near unity
271 ClNO_2 yield in Delhi (**Text S2.2 and Fig. S13a**).



272

273 **Fig. 1 Field characterization of N_2O_5 and ClNO_2 in Delhi.** Campaign-averaged diurnal variations
 274 of (a) N_2O_5 , (b) ClNO_2 , (c) NO, and (d) particulate Cl and gaseous HCl. Scatter plots of N_2O_5 versus
 275 ClNO_2 mixing ratios in (e) 2023 and (f) 2019, color-coded by the particulate Cl concentrations. The
 276 observation(Haslett et al., 2023) in 2019 is included for comparison, where the gaseous HCl
 277 measurement is not available. The right axis in (a) indicates solar radiation during the campaign in
 278 2023. The exact sunrise (07:07~07:15) time in 2019 is about 30 min later than that in 2023
 279 (06:55~06:32), while the sunset time in 2019 (17:24~18:03) is about 30 min earlier according to the
 280 records from timeanddate website. Gaseous HCl and particulate Cl measured by CIMS are also shown
 281 in (c). The upper and lower edge of the box and whisker in (a), (b) and (d) represent the 25th and 75th,
 282 and 10th and 90th percentiles, respectively. The dots and squares denote mean values and the lines inside
 283 the boxes indicate median levels. The shaded area in (a)-(d) indicates the 10th and 90th percentile range.

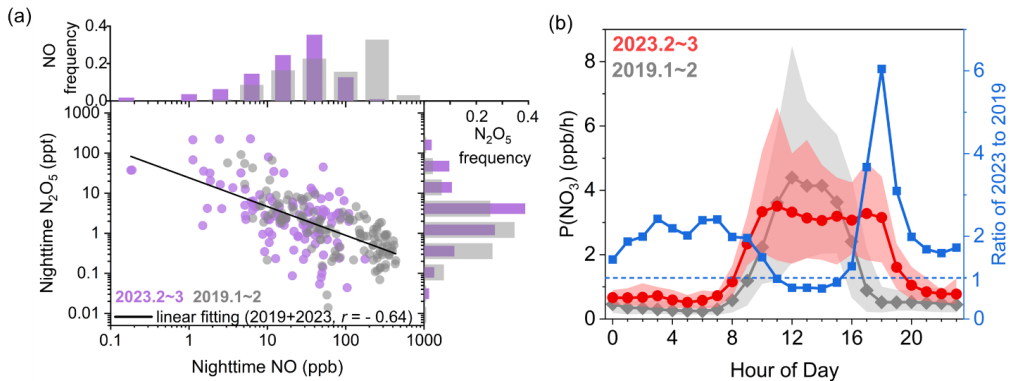
284



285 **3.2 Drivers of enhanced N₂O₅-ClNO₂ chemistry**

286 Lower NO concentrations in 2023 relative to 2019 reduce NO₃[·] losses to reactions with NO,
287 resulting in elevated nocturnal N₂O₅ levels. The reaction with NO dominated NO₃[·] losses both in 2019
288 and 2023 (~99%, **Fig. S7a**), contributing to the low abundances and short-lived occurrences of N₂O₅
289 in Delhi(Haslett et al., 2023). The strong anti-correlation between nocturnal N₂O₅ and NO persists in
290 2023, where the N₂O₅ mixing ratios overlap with those in 2019 when NO concentrations are within
291 the same range (approximately 2–100 ppb) (**Fig. 2a**). However, in 2023, the frequency of relatively
292 low-NO conditions (<2 ppb) rose from 0 to 8% and extreme NO levels (>100 ppb) nearly disappeared,
293 indicating that NO titration in suppressing N₂O₅ production has diminished (**Fig. 2a**). With the decline
294 in nighttime NO concentrations from 124 ± 25 ppb in 2019 to 44 ± 9 ppb ppb in 2023 (**Fig. 1c**),
295 the absolute NO₃[·] reactivity towards NO dropped by ~66% from 83.7 s⁻¹ to 28.4 s⁻¹, extending
296 nighttime NO₃[·] lifetimes approximately two folds in 2023 (0.04 s). The reduced NO₃[·] losses to NO
297 increased the availability of NO₃[·] for reacting with NO₂, thereby enhancing N₂O₅ production.
298 Additionally, no significant correlation between particulate Cl and ClNO₂ was observed in 2019, likely
299 because the chloride increases were accompanied by a substantial elevation in NO, which suppressed
300 N₂O₅ formation (**Fig. S9b**).

301 Higher NO₃[·] production rates (P(NO₃)) enhance N₂O₅ formation. Due to the increases in
302 nocturnal O₃ levels (from 3.5 to 6.8 ppb) and the reaction rate constant between NO₂ and O₃ (from
303 2.36×10^{-17} to 2.93×10^{-17} cm³ molec⁻¹ s⁻¹), the average nocturnal P(NO₃) in 2023 almost doubled
304 (0.75 ppb h⁻¹) compared to 2019 (0.41 ppb h⁻¹) (**Fig. 2b**). The observed (P(NO₃)) in Delhi 2023 exceeds
305 those reported in the United States(Wang et al., 2023b;Noxon et al., 1980) and Europe(Ljungström and
306 Hallquist, 1996;Wang et al., 2023b), and 1~2 times lower than those observed in China(Wang et al.,
307 2024;Yan et al., 2021;Chen et al., 2023). Consistently, the N₂O₅ mixing ratios in 2023 peak after sunset
308 around 18:00~19:00 (**Fig. 1a**), coinciding with the period of elevated P(NO₃) (**Fig. 2b**) and relatively
309 low NO levels (**Fig. 1c**). Other factors, such as the decreased aerosol surface area (2637±152 and
310 1411±162 μm²/cm³ in 2019 and 2023, respectively) results in reduced first-order heterogenous loss
311 rate coefficient of N₂O₅ (k_{het}) from 0.74±0.09 s⁻¹ in 2019 to 0.14±0.02 s⁻¹ in 2023, which also
312 contributes to the elevated nocturnal N₂O₅ mixing ratios observed in 2023. Overall, the enhanced
313 NO₃[·] production and reduced losses to NO led to elevated NO₃[·] and N₂O₅ levels in 2023, aligning
314 with the higher estimated steady-state NO₃[·] mixing ratios (0.25 ppt vs. 0.03 ppt in 2019) (**Fig. S7b**).
315 It should be emphasized that the 2019 and 2023 measurements were conducted in different seasons,
316 i.e., January to early February (winter) in 2019 and late February to mid-March (early spring) in 2023.
317 The observed increase in O₃ and decrease in NO and aerosol surface areas during the 2023 campaign
318 are influenced by the inter-month variability (e.g., change in boundary layer height and solar radiation)
319 of these pollutants (**Figs. S14a-b**).



320

321 **Fig. 2 Drivers of nocturnal N₂O₅ enhancement.** (a) Scatter plot of nighttime NO versus N₂O₅. The
322 top and right subfigures in (a) show the occurrence frequencies of NO and N₂O₅ in different
323 concentration bins, respectively. Nighttime is defined as the period from 20:00 to 04:00, excluding the
324 transition period between day and night when the air mass was unstable. (b) Campaign-averaged
325 diurnal variations of P(NO₃) in 2023 and 2019, respectively. The right axis in (b) displays the 2023-
326 to-2019 ratio of P(NO₃). The dots and squares denote mean values and the shaded area indicates the
327 10th and 90th percentile range.

328

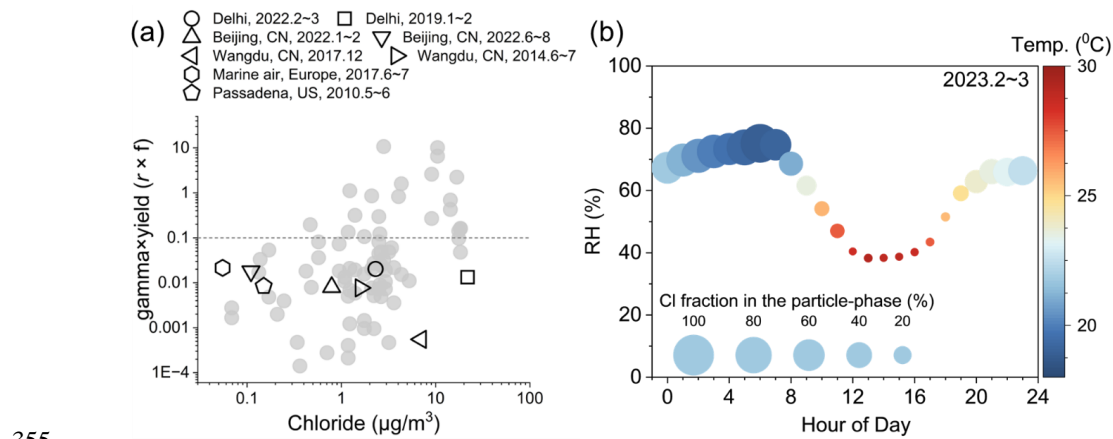
329 High particulate Cl concentrations drive significant N₂O₅ uptake and ClNO₂ production in Delhi.
330 The field-derived uptake parameter ($\gamma \times f$) in Delhi is similar with those observed in marine air (~ 0.02
331 on average)¹¹ and several times to an order of magnitude higher than those reported in other continental
332 regions ($6 \times 10^{-4} \sim 8 \times 10^{-3}$) (Xia et al., 2021; Tham et al., 2018; Xia et al., 2020; Mielke et al., 2013). As
333 is shown in **Fig. 3a**, this parameter increases with the particulate Cl level in Delhi, reflecting the
334 combined effects of chloride in promoting N₂O₅ uptake and ClNO₂ yield observed in prior laboratory
335 studies (Bertram and Thornton, 2009; Jahl et al., 2021). By contrast, despite comparable high chloride
336 ($\sim 6 \times 10^{-4}$ on average) and the nocturnal ClNO₂ level (typically < 50 ppt) are significantly lower than
337 those measured in Delhi. This is likely due to the lower ambient water content ($\sim 0.4\%$) compared to
338 Delhi ($\sim 1.5\%$), which limits aerosol liquid water content and thereby suppressed N₂O₅ hydrolysis on
339 particles (Xia et al., 2021; Tham et al., 2018).

340

341 The high chloride in Delhi is largely in the form of semi-volatile NH₄Cl, originating from gas to
342 particle partitioning. We observed a concurrent late-evening enrichment of non-refractory chloride
343 measured by CIMS and Cl element measured by XRF (**Fig. 1d**), indicating the semi-volatile nature of
344 particulate Cl (i.e., NH₄Cl) in Delhi. Additionally, direct measurements of both HCl and particulate Cl
345 enabled us to examine the gas–particle partitioning behavior of Cl. As shown in **Fig. 3b**, the particle-
346 phase Cl fraction amounted to up to 89% on average at 6:00 whereas it remained below 20% in the
347 afternoon (12:00–18:00). This diurnal variation is attributed to lower temperatures (15–25 °C) and



347 higher RH (56-92%) in the early morning hours, which favored the co-condensation of HCl and water
 348 vapor into particles as NH₄Cl under the NH₃-rich conditions commonly found in Delhi(Acharja et al.,
 349 2023;Gunthe et al., 2021). A recent study suggests that increasing RH promotes the migration of
 350 chloride from the particle bulk phase to the gas-particle interface (Fauré et al., 2024). This phenomenon
 351 helps explain the observed post-midnight accumulation of ClNO₂ and consistently low N₂O₅ levels in
 352 Delhi, which are attributed to enhanced heterogeneous conversion of N₂O₅ to ClNO₂ on aerosol
 353 surfaces. The observed thermodynamically-driven partitioning behavior of Cl agrees with previous
 354 model simulations (Gunthe et al., 2021;Chen et al., 2022b).



355 **Fig. 3 Drivers of nocturnal ClNO₂ enhancement in Delhi.** (a) Dependence of the field-observed
 356 uptake parameter ($\gamma \times f$) on particulate Cl concentrations in 2023. The campaign-average value for
 357 2023 (excluding unusually high values of $\gamma \times f > 0.1$) is shown as an open circle. The values derived
 358 from previous observations in Delhi 2019 (Haslett et al., 2023), Beijing (Chen et al., 2025b), Wangdu
 359 (Xia et al., 2021;Tham et al., 2018), Pasadena(Mielke et al., 2013), and marine air in Europe(Eger et
 360 al., 2019) are shown as different markers. The reference line of $\gamma \times f$ equals to 0.1 is also plotted. (b)
 361 Campaign-averaged diurnal variation of RH in 2023, color-coded by ambient temperature. The size of
 362 the datapoints is proportional to the observed Cl fraction in the particle-phase, which is calculated as
 363 $\text{Cl}_p/(\text{Cl}_p + \text{HCl}_g)$.

364 ClNO₂ levels in Delhi were influenced by the transport of ClNO₂-laden biomass burning plumes
 365 from upwind regions, and vertical intrusion associated with the breakup of the residual layer. We
 366 observed some cases with unusually high $\gamma \times f$ values exceeding 0.1(Tham et al., 2018), implying
 367 additional ClNO₂ sources beyond the local N₂O₅ uptake. Most of the high values were found during
 368 episodes of easterly (50~130°) winds with elevated particulate Cl concentrations (**Fig. 4a**), when the
 369 air masses passed over biomass-burning hotspots (**Fig. S15**). This suggests substantial ClNO₂
 370 production on high chloride containing biomass burning aerosols, as observed in previous laboratory
 371 experiments (Ahern et al., 2018;Jah et al., 2021). A typical case is shown in **Fig. S16**, where ClNO₂
 372

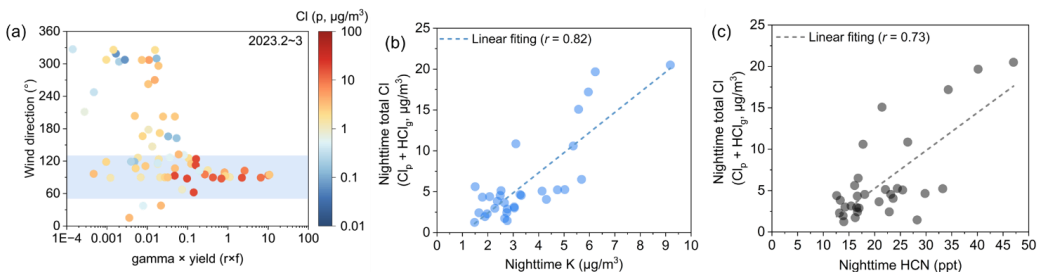


373 abruptly increases concurrently with the sharp rise in particulate Cl, biomass-burning tracers (K and
374 HCN, **Table S3**), and easterly wind speeds. Overall, the nighttime Cl strongly correlates with K ($r =$
375 0.82) and HCN ($r = 0.73$) (**Fig. 4b-c** and **Fig. S17**), indicating significant Cl emissions from biomass
376 burning in Delhi. The ambient nighttime Cl to K ratio (1.6 ± 0.8) in Delhi is about three-fold higher
377 (0.4 ± 0.2) than those measured from biomass/biofuel emission sources (**Table S3**), indicating
378 additional sources of Cl potentially from plastic-contained garbage burning, industrial processes, and
379 coal combustion (Gunthe et al., 2021). We consistently observed a moderate correlation between Cl
380 and the coal combustion tracer SO₂ ($r = 0.51$). In contrast, the poor correlation of total Cl with NO
381 ($r = -0.30$) and CO ($r = -0.08$) indicated limited contributions from vehicle exhaust, consistent with
382 their low Cl emission factors (**Table S3**). Additionally, a continued rise in ClNO₂ was observed after
383 sunrise (6:00~8:00; **Fig. 1b** and **Fig. S16**), likely due to the downward mixing of ClNO₂-rich air
384 masses aloft, as reported in other locations (Tham et al., 2016a; Haslett et al., 2023). We estimated that
385 108~805 ppt of ClNO₂ resided in the residual layer (**Text S3**), which is in the range (100~3000 ppt) of
386 previous measurements in polluted continental regions (Wang et al., 2017b; Wagner et al., 2012; Young
387 et al., 2012; Riedel et al., 2013). N₂O₅ and ClNO₂ production from NO_x, O₃, and chloride within the
388 residual layer can also contribute to the ground ClNO₂ levels (Wang et al., 2017b; Tham et al., 2016b),
389 but it is difficult to quantify in this study due to the lack of vertically-resolved measurements.

390 Since the above discussions are built on two short-term campaigns, we further assess the
391 prevalence of N₂O₅ and ClNO₂ production in Delhi based on the long-term distributions of the
392 identified driving factors, i.e., NO, P(NO₃), and particulate Cl (**Fig. S2**). The occurrence distribution
393 of nighttime NO and P(NO₃) during the 2023 campaign largely overlapped with the conditions
394 commonly occurred in Delhi (**Figs. S2a-b**), indicating comparable N₂O₅ production potential
395 throughout the years in Delhi. In addition, the frequency distribution of Cl_p in 2023 campaign is
396 comparable to that observed from January to April of 2022 and much higher than those reported from
397 May to September (**Fig. S2c**). The seasonal variation of chloride reflects the temperature-driven
398 evaporation of semi-volatile NH₄Cl as discussed previously. Given the critical role of Cl_p in promoting
399 N₂O₅ uptake and driving ClNO₂ production in Delhi, these results suggest that elevated nighttime N₂O₅
400 and ClNO₂ levels are most likely observed during the warm and cold seasons, respectively, in Delhi.

401

402



403

404 **Fig. 4 The key source of Cl emission in Delhi.** (a) Scatter plot of uptake parameter ($\gamma \times f$) and wind
 405 direction color-coded by particulate Cl concentrations. The shaded area in (a) indicates the region with
 406 wind direction ranging from 50° to 130°. Correlation of nocturnal total Cl (sum of Cl_p and HCl_g) with
 407 (b) particulate K and (c) gaseous HCN. The reported HCN mixing ratio can be considered a lower-
 408 limit estimate (see **Methods 2.1**).

409

3.3 Impacts on atmospheric radical production and VOCs oxidation

410 Enhanced $\text{N}_2\text{O}_5\text{-ClNO}_2$ chemistry at lower NO levels emphasizes the important roles of $\text{Cl}\cdot$ and
 411 $\text{NO}_3\cdot$ in initiating the oxidation of VOCs in Delhi. The average daytime Cl production rate ($P(\text{Cl})$)
 412 from ClNO_2 photolysis in 2023 (0.035 ppb/h) is about approximately twice that observed in 2019
 413 (0.015 ppb/h). The maximum daytime-averaged $P(\text{Cl})$ (0.24 ppb/h) from the photolysis of all the
 414 detected $\text{Cl}\cdot$ precursors (Cl_2 , ClNO_2 , NHCl_2 , and NCl_3) is up to an order of magnitude higher than
 415 values reported for the urban inland areas of Europe and North America (0.02~0.07 ppb/h)(Priestley
 416 et al., 2018;McNamara et al., 2020;Faxon et al., 2015), and remains several times lower than those
 417 observed during the pollution episodes in China (0.5~1.1 ppb/h) (Chen et al., 2023;Tham et al.,
 418 2016b;Liu et al., 2017). ClNO_2 photolysis dominates the production of $\text{Cl}\cdot$ around the sunrise hours
 419 (7:00~8:00) when the $P(\text{Cl})_{\text{total}}$ to $P(\text{OH})$ ratio (42 on average) was also the highest (**Fig. 5a**), suggesting
 420 pronounced Cl-initiated oxidation of VOCs under these conditions in Delhi.

421

422 Consistently, we observed specific gaseous organic oxidation products indicative of the
 423 prevalence of chlorine chemistry (**Fig. 5b**). We identified organochlorinated species, i.e., $\text{C}_2\text{H}_3\text{O}_2\text{Cl}$
 424 and $\text{C}_3\text{H}_5\text{O}_2\text{Cl}$ (presumably chloroacetic acid and chloropropionic acid), which were previously
 425 measured in chamber experiments from $\text{Cl}\cdot$ reacting with ethylbenzene (Jahn et al., 2024) and isoprene
 426 (Wang et al., 2022) and used as markers for the occurrence of chlorine chemistry in field studies
 427 (Priestley et al., 2018;Li et al., 2025). The daytime concentration fraction of $\text{C}_2\text{H}_3\text{O}_2\text{Cl}$ in the total
 428 measured gaseous organics increases from ~0.9% in 2019 to ~1.8% in 2023. Additionally, the daytime
 429 average peak mixing ratio of $\text{C}_2\text{H}_3\text{O}_2\text{Cl}$ (~100 ppt) in 2023 is about 5~30 times higher than those
 430 measured in Hong Kong (12~20 ppt) (Li et al., 2025) and Manchester (~3 ppt) (Priestley et al., 2018),
 431 indicating significant $\text{C}_2\text{H}_3\text{ClO}_2$ production in Delhi. We also identified a series of hydroxynitrates
 432 (HN) homologues, i.e., $\text{C}_8\text{H}_{17}\text{O}_4\text{N}$, $\text{C}_{10}\text{H}_{21}\text{O}_4\text{N}$, and $\text{C}_{12}\text{H}_{25}\text{O}_4\text{N}$, which were potentially early-
 433 generation products from the chlorine-initiated oxidation of $\text{C}_{8,10,12}$ -alkanes under high NO_x conditions



433 (Wang and Hildebrandt Ruiz, 2018). Here their sharp increase in the early morning hours (7:00~8:00)
434 when $\text{Cl}\cdot$ was likely the dominant atmospheric oxidant (**Figs. 5a-b**), together with the positive
435 correlations between these HN and the product of $\text{P}(\text{Cl})$ and NO ($r_{7:00\sim8:00} = 0.59$, **Fig. 5e**), underscores
436 the $\text{Cl}\cdot$ initiated alkane oxidation in the presence of NO as an important source of HN in Delhi. It is
437 noted that these HN can also be formed via OH-initiated oxidation processes (Lim and Ziemann, 2009),
438 but would then likely peak later in the day when OH concentrations are higher. Here, a quantitative
439 comparison between the $\text{Cl}\cdot$ and OH-initiated reaction pathways is missing in current study due to the
440 lack of VOCs precursor measurements and warrants further investigation.

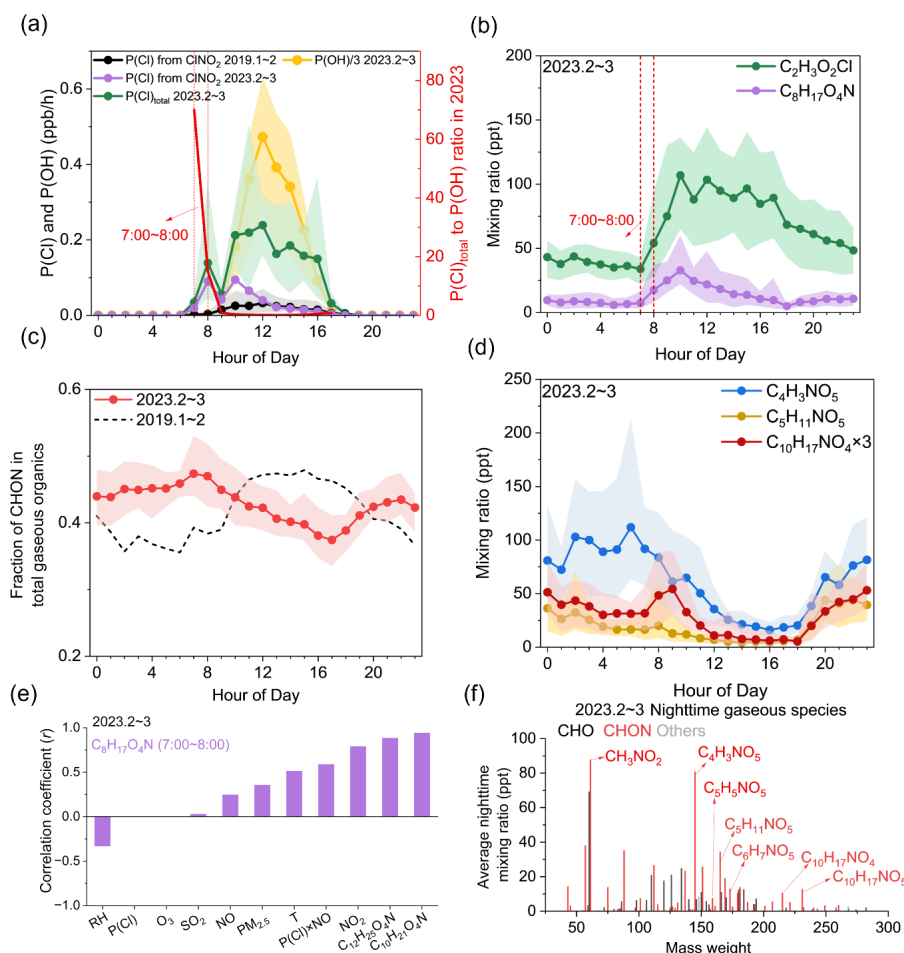
441 The $\text{NO}_3\cdot$ -initiated nocturnal oxidation of VOCs was strengthened during the 2023 campaign. The
442 fraction of nitrogen-containing organics (CHON) in the total measured gaseous oxygenated organic
443 compounds in 2023 (~46%) was similar to that observed in 2019 (42%). However, the diurnal pattern
444 of the CHON fraction was inversed, exhibiting a moderate increase (~9%) during the nighttime (**Fig.**
445 **5c**), which resembles those found in other locations (Ye et al., 2021;Huang et al., 2019), indicating
446 enhanced nocturnal $\text{NO}_3\cdot$ -driven organic oxidation in 2023. We further identified the nighttime gaseous
447 organic species with the criteria of average nighttime (20:00~04:00) to daytime (7:00~16:00) mixing
448 ratio larger than 1. Most of the nighttime species are nitrogen-containing compounds, primarily
449 including $\text{C}_{4,5,6}\text{H}_{3,5,7}\text{O}_5\text{N}$ and $\text{C}_{10}\text{H}_{17}\text{O}_{4,5}\text{N}$ (**Fig. 5f**), which are typical first-generation oxidation
450 products from $\text{NO}_3\cdot$ -induced oxidation of heterocyclics (i.e., furan, methylfuran, and dimethylfuran)
451 (Chen et al., 2022a;Joo et al., 2019;Jiang et al., 2020) and monoterpenes (Jenks et al., 2023;Ayres et
452 al., 2015), respectively. These oxidation products exhibited strong intra-group correlations ($r_{20:00\sim4:00}$
453 = 0.71 to 0.77), whereas the correlations between the $\text{C}_{4,5,6}\text{H}_{3,5,7}\text{O}_5\text{N}$ and $\text{C}_{10}\text{H}_{17}\text{O}_{4,5}\text{N}$ groups were
454 weak ($r_{20:00\sim4:00} < 0.2$), confirming their production from distinct precursors. Moreover, their low
455 correlations with CO and NO ($r_{20:00\sim4:00} < 0.4$) largely exclude direct combustion emissions as the
456 dominant source. Notably, observations of furan-derived $\text{NO}_3\cdot$ oxidation products have currently been
457 limited to laboratory studies (Chen et al., 2022a;Joo et al., 2019;Jiang et al., 2020). Our findings offer
458 direct field evidence of $\text{NO}_3\cdot$ -initiated furan oxidation in the atmosphere.

459 Another prominent nighttime compound potentially associated with $\text{NO}_3\cdot$ induced oxidation is
460 $\text{C}_5\text{H}_{11}\text{NO}_5$ (**Fig. 5f**), which exhibited the largest nocturnal enhancement among all the observed species,
461 increasing by a factor of 3.6. $\text{C}_5\text{H}_{11}\text{NO}_5$ correlates well with $\text{C}_{10}\text{H}_{17}\text{O}_5\text{N}$ ($r_{20:00\sim4:00} = 0.71$) and shows
462 a marked increase between 18:00 and 19:00 (**Fig. 5d**), coinciding with the peak of the estimated
463 $\text{NO}_3\cdot$ levels (~2.3 ppt) (**Fig. S7b**). It is thus likely a co-product from the reaction of $\text{NO}_3\cdot$ with
464 monoterpenes. However, this compound has not been reported from any $\text{NO}_3\cdot$ -initiated oxidation
465 processes (Jenks et al., 2023;Ayres et al., 2015;Xu et al., 2025). Further investigation is required to
466 elucidate the formation mechanisms of $\text{C}_5\text{H}_{11}\text{NO}_5$ in Delhi's atmosphere.

467 In addition to the specific organic products discussed above, the overall oxidation state of the
468 measured organic aerosols (OA) is elevated in 2023 compared to 2019. The bulk oxygen-to-carbon



469 (O/C) ratio of OA (0.76 on average) was higher than the value (0.66) reported in the 2019 campaign
 470 (Huang et al., 2024), indicating an increased contribution from more oxidized or aged secondary
 471 organic aerosols (SOA) (Jimenez et al., 2009). A clear negative dependence of the O/C ratio on NO
 472 was observed at night when NO exceeded about 10 ppb (Figs. S18a-b), agreeing with the suppression
 473 effect of NO on organic oxidation by increasing the competitive $\text{RO}_2 + \text{NO}$ channel under the radical-
 474 limited regime commonly found in Delhi (Nelson et al., 2021;Kenagy et al., 2024). Taken together, the
 475 characteristics of the bulk organics provide additional field evidence for the enhanced atmospheric
 476 organics oxidation in 2023.

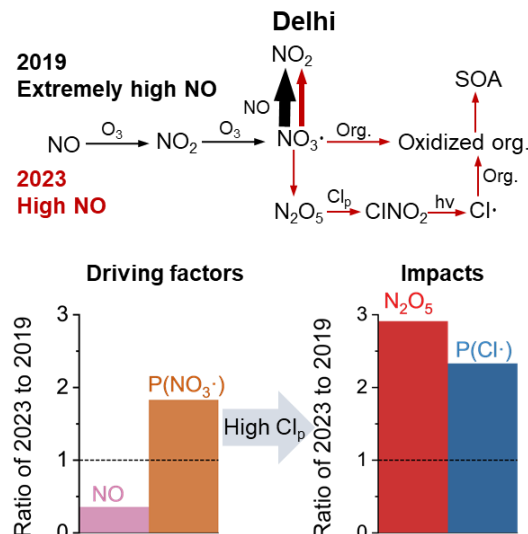


477

478 **Fig. 5 Enhanced daytime $\text{Cl}\cdot$ and nocturnal $\text{NO}_3\cdot$ initiated oxidation of organics in Delhi.** (a) $\text{P}(\text{Cl})$
 479 in 2023 and 2019, and $\text{P}(\text{OH})$ from the photolysis of O_3 in 2023. The $\text{P}(\text{Cl})_{\text{total}}$ 2023 includes
 480 $\text{Cl}\cdot$ production from the sum of ClNO_2 , Cl_2 , NHCl_2 , and NCl_3 photolysis. The $\text{P}(\text{Cl})_{\text{total}}$ to $\text{P}(\text{OH})$ ratio
 481 in 2023 is shown in the right axis. The value of $\text{P}(\text{OH})$ is divided by a factor of 3 to place it on the



482 same scale as $P(Cl)$. Average diurnal variations of tracer compounds indicating (b) $Cl\cdot$ and (d)
483 $NO_3\cdot$ initiated oxidation, respectively. (c) Comparison of the diurnal variations of CHON compounds
484 fraction in total detected gaseous organics in 2019 and 2023. (e) Correlation coefficients, using
485 observations between 7:00 and 8:00 of $C_8H_{17}NO_4$ with $P(Cl)_{total}$, meteorological parameters, trace
486 gases, and related homologue species. (f) Molecular composition and average nighttime mixing ratios
487 for the nighttime gaseous species. The shaded area in (a-d) indicates the 10th and 90th percentiles and
488 the dots denote mean values.



489
490 **Fig. 6 Amplified N_2O_5 and $ClNO_2$ production and impacts on secondary organic aerosol**
491 **formation in Delhi.** A schematic comparing N_2O_5 - $ClNO_2$ chemistry between the 2019 and 2023
492 campaigns. Red arrows indicate reactions that are largely enhanced during the 2023 campaign.

493 4 Conclusions

494 This study provides an extensive characterization of N_2O_5 - $ClNO_2$ chemistry in Delhi (Fig. 6). We
495 observed a clear dependency on available nocturnal NO that high NO suppresses N_2O_5 production and
496 reduces the formation of $ClNO_2$ while decreased NO promotes nocturnal N_2O_5 - $ClNO_2$ chemistry. The
497 former pattern is consistent with the previously reported significant NO suppression in 2019 (Haslett
498 et al., 2023). With moderate NO in 2023, substantial $ClNO_2$ is produced after midnight hours in Delhi,
499 which is driven by the elevated RH and chloride levels that promote efficient conversion of N_2O_5 to
500 $ClNO_2$. The abundance of chloride strongly correlates with the biomass burning tracers, indicating
501 emissions from biomass burning as an important source of Cl in Delhi. The increased $ClNO_2$ levels at
502 lower nocturnal NO conditions implies that the atmospheric oxidation of organics is amplified both
503 during the nighttime (via $NO_3\cdot$ pathways) and daytime (via $Cl\cdot$ pathways) in Delhi.



504 The differing behaviors of N_2O_5 and ClNO_2 depending on the levels of nocturnal NO emphasize
505 the need of continuous monitoring of air pollutants in Delhi, which is essential to understand the
506 evolution of emission sources and atmospheric chemical processes. The complexity of the air pollution
507 situation in Delhi has been further scrutinized where we noted that as chloride levels declined, nitrate
508 has become the leading inorganic component since late 2019 (**Figs. S3a-b**) and plays an increasingly
509 important role in exacerbating Delhi's $\text{PM}_{2.5}$ pollution (**Fig. S3c**). Thus, future studies should pay
510 attention to elucidating the dominant production pathways of nitrate in Delhi, especially the
511 contribution from N_2O_5 heterogeneous hydrolysis (Wang et al., 2017a; Yan et al., 2023).

512 The present study suggests that NO_x emission control may intensify atmospheric oxidation of
513 organics and secondary organic aerosol (SOA) formation in Delhi, whereas concurrent chlorine
514 emission regulations may help mitigate the associated negative impacts. Despite recent reductions, the
515 chloride concentrations in Delhi remain among the highest reported worldwide (**Fig. S1a**). Previous
516 studies have revealed the critical role chloride has in exacerbating haze formation in Delhi by
517 enhancing aerosol liquid water content (ALWC) (Chen et al., 2022b; Gunthe et al., 2021), while our
518 study implies that, with the decrease in NO concentrations, chloride can also be readily activated into
519 photolabile gases, contributing to the formation of secondary pollutant, e.g., SOA, through generating
520 radicals and advancing atmospheric organics oxidation. Chloride is mostly of anthropogenic origins in
521 Delhi (Sharma et al., 2019; Gunthe et al., 2021) and we identified biomass burning as one of the major
522 sources of chlorine during our measurements. It is expected that regulations on biomass burning along
523 with transition to clean residential fuels (e.g., natural gas and electricity) would benefit $\text{PM}_{2.5}$
524 abatement in Delhi by not only cutting primary particle emissions, but also suppressing secondary
525 pollutant formation. To support such strategies, an updated chlorine emission inventory combined with
526 modelling studies, is necessary to quantitatively evaluate the contribution of chlorine chemistry to
527 $\text{PM}_{2.5}$ formation under different NO_x reduction scenarios and inform targeted emission control
528 strategies. Finally, the interplay between nitrogen and halogen chemistry in India warrants continued
529 investigation in the context of ongoing industrialization, vehicle electrification, and a changing climate.

530 **Supporting Information**

531 Text S1 to S3, Table S1 to S3 and Figs. S1 to S20

532 **Acknowledgments**

533 We acknowledge financial support from National Natural Science Foundation of China (grant no.
534 22188102), Tsinghua Scholarship for Overseas Graduate Studies (contract no. 2023012), Swedish
535 Research Council (grant no. 2023-045209), the Swedish Research Council for Sustainable
536 Development (grant no. 2020-02009 and 2022-01441) and the Swedish Strategic Research Area
537 MERGE (Modelling the Regional and Global Earth System). Nishu Sachdeva and Johan Boman from
538 University of Gothenburg are gratefully acknowledged for their contributions to the EDXRF analyses.



539 **Data Availability**

540 The dataset used for this study is available at <https://cloud.tsinghua.edu.cn/d/cb099983b459474fa1df/>.
541 Measurement data from the Sri Aurobindo Marg monitoring station in Delhi is available at
542 <https://www.dpccairdata.com/dpccairdata/display/AallAdvanceSearchMet.php?stName=U3JpQXVY>
543 YmluZG9NYXJn. The Tropospheric Ultraviolet and Visible Radiation (TUV) Model is accessible at
544 https://www.acom.ucar.edu/Models/TUV/Interactive_TUV. The exact sunrise and sunset time during
545 the 2023 and 2019 campaign are retrieved from the website
546 <https://www.timeanddate.com/sun/india/delhi>.

547 **Author Contributions**

548 M.H., Y.C., C.W., and J.J. designed the study. E.T., J.P., C.W., R.P., and M.H. organized and performed
549 the field observations in Delhi. R.P., H.M., G.H., and G.T. provided the measurement space, helped
550 setting up the instruments, and facilitated the measurements. Y.C., E.T. and J.P. calibrated and
551 quantified the data. Y.C. analyzed and visualized the data. Y.C. wrote the original draft with inputs
552 from J.J., M.H., and C.W. All co-authors contributed to scientific discussions and reviewing the
553 manuscript.

554 **Author Information**

555 The authors declare no competing financial interests.

556 **References**

557 Acharja, P., Ghude, S. D., Sinha, B., Barth, M., Govardhan, G., Kulkarni, R., Sinha, V., Kumar, R., Ali,
558 K., Gultepe, I., Petit, J.-E., and Rajeevan, M. N.: Thermodynamical framework for effective mitigation
559 of high aerosol loading in the Indo-Gangetic Plain during winter, *Scientific Reports*, 13, 13667,
560 <https://doi.org/10.1038/s41598-023-40657-w>, 2023.

561 Aggarwal, S., Bansal, P., Wang, Y., Jorga, S., Macgregor, G., Rohner, U., Bannan, T., Salter, M., Zieger,
562 P., Mohr, C., and Lopez-Hilfiker, F.: Identifying key parameters that affect sensitivity of flow tube
563 chemical ionization mass spectrometers, *Atmos. Meas. Tech.*, 18, 4227-4247,
564 <https://doi.org/10.5194/amt-18-4227-2025>, 2025.

565 Ahern, A. T., Goldberger, L., Jahl, L., Thornton, J., and Sullivan, R. C.: Production of N₂O₅ and ClNO₂
566 through Nocturnal Processing of Biomass-Burning Aerosol, *Environ. Sci. Technol.*, 52, 550-559,
567 <https://doi.org/10.1021/acs.est.7b04386>, 2018.

568 Ayres, B. R., Allen, H. M., Draper, D. C., Brown, S. S., Wild, R. J., Jimenez, J. L., Day, D. A.,
569 Campuzano-Jost, P., Hu, W., de Gouw, J., Koss, A., Cohen, R. C., Duffey, K. C., Romer, P., Baumann,
570 K., Edgerton, E., Takahama, S., Thornton, J. A., Lee, B. H., Lopez-Hilfiker, F. D., Mohr, C., Wennberg,
571 P. O., Nguyen, T. B., Teng, A., Goldstein, A. H., Olson, K., and Fry, J. L.: Organic nitrate aerosol
572 formation via NO₃ + biogenic volatile organic compounds in the southeastern United States, *Atmos.*
573 *Chem. Phys.*, 15, 13377-13392, <https://doi.org/10.5194/acp-15-13377-2015>, 2015.

574 Bannan, T. J., Booth, A. M., Bacak, A., Muller, J. B. A., Leather, K. E., Le Breton, M., Jones, B., Young,
575 D., Coe, H., Allan, J., Visser, S., Slowik, J. G., Furger, M., Prévôt, A. S. H., Lee, J., Dunmore, R. E.,



576 Hopkins, J. R., Hamilton, J. F., Lewis, A. C., Whalley, L. K., Sharp, T., Stone, D., Heard, D. E., Fleming,
577 Z. L., Leigh, R., Shallcross, D. E., and Percival, C. J.: The first UK measurements of nitryl chloride
578 using a chemical ionization mass spectrometer in central London in the summer of 2012, and an
579 investigation of the role of Cl atom oxidation, *Journal of Geophysical Research: Atmospheres*, 120,
580 5638-5657, <https://doi.org/10.1002/2014jd022629>, 2015.

581 Bertram, T. H., and Thornton, J. A.: Toward a general parameterization of N_2O_5 reactivity on aqueous
582 particles: the competing effects of particle liquid water, nitrate and chloride, *Atmos. Chem. Phys.*, 9,
583 8351-8363, <https://doi.org/10.5194/acp-9-8351-2009>, 2009.

584 Brown, S. S., and Stutz, J.: Nighttime radical observations and chemistry, *Chemical Society Reviews*,
585 41, 6405-6447, <https://doi.org/10.1039/C2CS35181A>, 2012.

586 Bryant, D. J., Nelson, B. S., Swift, S. J., Budisulistiorini, S. H., Drysdale, W. S., Vaughan, A. R.,
587 Newland, M. J., Hopkins, J. R., Cash, J. M., Langford, B., Nemitz, E., Acton, W. J. F., Hewitt, C. N.,
588 Mandal, T., Gurjar, B. R., Shivani, Gadi, R., Lee, J. D., Rickard, A. R., and Hamilton, J. F.: Biogenic
589 and anthropogenic sources of isoprene and monoterpenes and their secondary organic aerosol in Delhi,
590 India, *Atmos. Chem. Phys.*, 23, 61-83, <https://doi.org/10.5194/acp-23-61-2023>, 2023.

591 Burkholder, J., Sander, S., Abbatt, J., Barker, J., Cappa, C., Crounse, J., Dibble, T., Huie, R., Kolb, C.,
592 and Kurylo, M.: Chemical Kinetics and Photochemical Data for Use in Atmospheric Studies
593 Evaluation Number 19, JPL Publication 19-5, Jet Propulsion Laboratory, 2020.

594 Chen, K., Mayorga, R., Raeofy, N., Lum, M., Woods, M., Bahreini, R., Zhang, H., and Lin, Y.-H.:
595 Effects of Nitrate Radical Levels and Pre-Existing Particles on Secondary Brown Carbon Formation
596 from Nighttime Oxidation of Furan, *ACS Earth and Space Chemistry*, 6, 2709-2721,
597 <https://doi.org/10.1021/acsearthspacechem.2c00244>, 2022a.

598 Chen, X., Xia, M., Wang, W., Yun, H., Yue, D., and Wang, T.: Fast near-surface ClNO_2 production and
599 its impact on O_3 formation during a heavy pollution event in South China, *Sci Total Environ*, 858,
600 159998, <https://doi.org/10.1016/j.scitotenv.2022.159998>, 2023.

601 Chen, X., Jiang, Y., Zong, Z., Wang, Y., Sun, W., Wang, Y., Xia, M., Guan, L., Liu, P., Zhang, C., Chen,
602 J., Mu, Y., and Wang, T.: Atmospheric Reactive Halogens Reshaped by the Clean Energy Policy and
603 Agricultural Activity in a Rural Area of the North China Plain, *Environmental Science & Technology*,
604 <https://doi.org/10.1021/acs.est.4c13986>, 2025a.

605 Chen, Y., Wang, Y., Nenes, A., Wild, O., Song, S., Hu, D., Liu, D., He, J., Hildebrandt Ruiz, L., Apte,
606 J. S., Gunthe, S. S., and Liu, P.: Ammonium Chloride Associated Aerosol Liquid Water Enhances Haze
607 in Delhi, India, *Environ Sci Technol*, <https://doi.org/10.1021/acs.est.2c00650>, 2022b.

608 Chen, Y., Xia, M., Zhang, J., Tsiligiannis, E., Wu, C., Yan, C., Cai, R., Zheng, G., Li, Y., Guo, J., An,
609 Z., Li, Y., Zhao, X., Qu, Q., Hua, C., Wang, Z., Wang, S., Liu, Y., Cao, L., He, K., Kulmala, M.,
610 Hallquist, M., Wang, T., Worsnop, D., and Jiang, J.: Chloramine chemistry as a missing link in
611 atmospheric chlorine cycling, *Science Advances*, 11, eadv4298,
612 <https://doi.org/10.1126/sciadv.adv4298>, 2025b.

613 Dentener, F. J., and Crutzen, P. J.: Reaction of N_2O_5 on tropospheric aerosols: Impact on the global
614 distributions of NO_x , O_3 , and OH , *Journal of Geophysical Research: Atmospheres*, 98, 7149-7163,
615 <https://doi.org/https://doi.org/10.1029/92JD02979>, 1993.

616 Dunlea, E. J., and Ravishankara, A.: Measurement of the rate coefficient for the reaction of $\text{O}({}^1\text{D})$ with



617 H₂O and re-evaluation of the atmospheric OH production rate, *Physical Chemistry Chemical Physics*,
618 6, 3333-3340, 2004.

619 Eger, P. G., Friedrich, N., Schuladen, J., Shenolikar, J., Fischer, H., Tadic, I., Harder, H., Martinez, M.,
620 Rohloff, R., Tauer, S., Drewnick, F., Fachinger, F., Brooks, J., Darbyshire, E., Sciare, J., Pikridas, M.,
621 Lelieveld, J., and Crowley, J. N.: Shipborne measurements of ClNO₂ in the Mediterranean Sea and
622 around the Arabian Peninsula during summer, *Atmospheric Chemistry and Physics*, 19, 12121-12140,
623 <https://doi.org/10.5194/acp-19-12121-2019>, 2019.

624 Evans, M. J., and Jacob, D. J.: Impact of new laboratory studies of N₂O₅ hydrolysis on global model
625 budgets of tropospheric nitrogen oxides, ozone, and OH, *Geophysical Research Letters*, 32,
626 <https://doi.org/https://doi.org/10.1029/2005GL022469>, 2005.

627 Fauré, N., Chen, J., Artiglia, L., Ammann, M., Bartels-Rausch, T., Kanji, Z. A., Wang, S., Pettersson,
628 J. B. C., Thomson, E. S., Gladich, I., and Kong, X.: Formation of Sodium Chloride on the Surface of
629 Sulfate-Rich Gobi Desert Salt in Response to Water Adsorption, *ACS ES&T Air*, 1, 1373-1382,
630 <https://doi.org/10.1021/acs.estair.4c00092>, 2024.

631 Faxon, C., Bean, J., and Ruiz, L.: Inland Concentrations of Cl₂ and ClNO₂ in Southeast Texas Suggest
632 Chlorine Chemistry Significantly Contributes to Atmospheric Reactivity, *Atmosphere*, 6, 1487-1506,
633 <https://doi.org/10.3390/atmos6101487>, 2015.

634 Finlayson-Pitts, B. J., Ezell, M. J., and Pitts, J. N.: Formation of chemically active chlorine compounds
635 by reactions of atmospheric NaCl particles with gaseous N₂O₅ and ClONO₂, *Nature*, 337, 241-244,
636 <https://doi.org/10.1038/337241a0>, 1989.

637 Gani, S., Bhandari, S., Patel, K., Seraj, S., Soni, P., Arub, Z., Habib, G., Hildebrandt Ruiz, L., and Apte,
638 J. S.: Particle number concentrations and size distribution in a polluted megacity: the Delhi Aerosol
639 Supersite study, *Atmos. Chem. Phys.*, 20, 8533-8549, <https://doi.org/10.5194/acp-20-8533-2020>, 2020.

640 Gunthe, S. S., Liu, P., Panda, U., Raj, S. S., Sharma, A., Darbyshire, E., Reyes-Villegas, E., Allan, J.,
641 Chen, Y., Wang, X., Song, S., Pöhlker, M. L., Shi, L., Wang, Y., Kommula, S. M., Liu, T., Ravikrishna,
642 R., McFiggans, G., Mickley, L. J., Martin, S. T., Pöschl, U., Andreae, M. O., and Coe, H.: Enhanced
643 aerosol particle growth sustained by high continental chlorine emission in India, *Nature Geoscience*,
644 14, 77-84, <https://doi.org/10.1038/s41561-020-00677-x>, 2021.

645 Haslett, S. L., Bell, D. M., Kumar, V., Slowik, J. G., Wang, D. S., Mishra, S., Rastogi, N., Singh, A.,
646 Ganguly, D., Thornton, J., Zheng, F., Li, Y., Nie, W., Liu, Y., Ma, W., Yan, C., Kulmala, M.,
647 Daellenbach, K. R., Hadden, D., Baltensperger, U., Prevot, A. S. H., Tripathi, S. N., and Mohr, C.:
648 Nighttime NO emissions strongly suppress chlorine and nitrate radical formation during the winter in
649 Delhi, *Atmos. Chem. Phys.*, 23, 9023-9036, <https://doi.org/10.5194/acp-23-9023-2023>, 2023.

650 Huang, W., Saathoff, H., Shen, X., Ramisetty, R., Leisner, T., and Mohr, C.: Chemical Characterization
651 of Highly Functionalized Organonitrates Contributing to Night-Time Organic Aerosol Mass Loadings
652 and Particle Growth, *Environmental Science & Technology*, 53, 1165-1174,
653 <https://doi.org/10.1021/acs.est.8b05826>, 2019.

654 Huang, W., Wu, C., Gao, L., Gramlich, Y., Haslett, S. L., Thornton, J., Lopez-Hilfiker, F. D., Lee, B.
655 H., Song, J., Saathoff, H., Shen, X., Ramisetty, R., Tripathi, S. N., Ganguly, D., Jiang, F., Vallon, M.,
656 Schobesberger, S., Yli-Juuti, T., and Mohr, C.: Variation in chemical composition and volatility of
657 oxygenated organic aerosol in different rural, urban, and mountain environments, *Atmos. Chem. Phys.*,



658 24, 2607-2624, <https://doi.org/10.5194/acp-24-2607-2024>, 2024.

659 Jahl, L. G., Bowers, B. B., Jahn, L. G., Thornton, J. A., and Sullivan, R. C.: Response of the Reaction
660 Probability of N₂O₅ with Authentic Biomass-Burning Aerosol to High Relative Humidity, *ACS Earth*
661 *and Space Chemistry*, 5, 2587-2598, <https://doi.org/10.1021/acsearthspacechem.1c00227>, 2021.

662 Jahn, L. G., McPherson, K. N., and Hildebrandt Ruiz, L.: Effects of Relative Humidity and Photoaging
663 on the Formation, Composition, and Aging of Ethylbenzene SOA: Insights from Chamber Experiments
664 on Chlorine Radical-Initiated Oxidation of Ethylbenzene, *ACS Earth and Space Chemistry*, 8, 675-
665 688, <https://doi.org/10.1021/acsearthspacechem.3c00279>, 2024.

666 Jenks, O. J., DeVault, M. P., Ziola, A. C., Morris, M. A., Schueneman, M. K., Stark, H., Jimenez, J. L.,
667 Ziemann, P. J., and de Gouw, J. A.: Investigation of Gas-Phase Products from the NO₃ Radical
668 Oxidation of Δ-3-Carene, *ACS Earth and Space Chemistry*, 7, 1097-1106,
669 <https://doi.org/10.1021/acsearthspacechem.3c00020>, 2023.

670 Jiang, J., Carter, W. P. L., Cocker, D. R., III, and Barsanti, K. C.: Development and Evaluation of a
671 Detailed Mechanism for Gas-Phase Atmospheric Reactions of Furans, *ACS Earth and Space
672 Chemistry*, 4, 1254-1268, <https://doi.org/10.1021/acsearthspacechem.0c00058>, 2020.

673 Jimenez, J. L., Canagaratna, M. R., Donahue, N. M., Prevot, A. S. H., Zhang, Q., Kroll, J. H., DeCarlo,
674 P. F., Allan, J. D., Coe, H., Ng, N. L., Aiken, A. C., Docherty, K. S., Ulbrich, I. M., Grieshop, A. P.,
675 Robinson, A. L., Duplissy, J., Smith, J. D., Wilson, K. R., Lanz, V. A., Hueglin, C., Sun, Y. L., Tian, J.,
676 Laaksonen, A., Raatikainen, T., Rautiainen, J., Vaattovaara, P., Ehn, M., Kulmala, M., Tomlinson, J.,
677 Collins, D. R., Cubison, M. J., E., Dunlea, J., Huffman, J. A., Onasch, T. B., Alfarra, M. R.,
678 Williams, P. I., Bower, K., Kondo, Y., Schneider, J., Drewnick, F., Borrmann, S., Weimer, S., Demerjian,
679 K., Salcedo, D., Cottrell, L., Griffin, R., Takami, A., Miyoshi, T., Hatakeyama, S., Shimono, A., Sun,
680 J. Y., Zhang, Y. M., Dzepina, K., Kimmel, J. R., Sueper, D., Jayne, J. T., Herndon, S. C., Trimborn, A.,
681 M., Williams, L. R., Wood, E. C., Middlebrook, A. M., Kolb, C. E., Baltensperger, U., and Worsnop,
682 D. R.: Evolution of Organic Aerosols in the Atmosphere, *Science*, 326, 1525-1529,
683 <https://doi.org/doi:10.1126/science.1180353>, 2009.

684 Joo, T., Rivera-Rios, J. C., Takeuchi, M., Alvarado, M. J., and Ng, N. L.: Secondary Organic Aerosol
685 Formation from Reaction of 3-Methylfuran with Nitrate Radicals, *ACS Earth and Space Chemistry*, 3,
686 922-934, <https://doi.org/10.1021/acsearthspacechem.9b00068>, 2019.

687 Kashyap, P., Kumar, A., Kumar, R. P., and Kumar, K.: Biogenic and anthropogenic isoprene emissions
688 in the subtropical urban atmosphere of Delhi, *Atmospheric Pollution Research*, 10, 1691-1698,
689 <https://doi.org/https://doi.org/10.1016/j.apr.2019.07.004>, 2019.

690 Kenagy, H. S., Heald, C. L., Tahsini, N., Goss, M. B., and Kroll, J. H.: Can we achieve atmospheric
691 chemical environments in the laboratory? An integrated model-measurement approach to chamber
692 SOA studies, *Science Advances*, 10, eado1482, <https://doi.org/10.1126/sciadv.ado1482>, 2024.

693 Kercher, J. P., Riedel, T. P., and Thornton, J. A.: Chlorine activation by N₂O₅: simultaneous, in situ
694 detection of ClNO₂ and N₂O₅ by chemical ionization mass spectrometry, *Atmos. Meas. Tech.*, 2, 193-
695 204, <https://doi.org/10.5194/amt-2-193-2009>, 2009.

696 Kumar, V., Giannoukos, S., Haslett, S. L., Tong, Y., Singh, A., Bertrand, A., Lee, C. P., Wang, D. S.,
697 Bhattu, D., Stefenelli, G., Dave, J. S., Puthussery, J. V., Qi, L., Vats, P., Rai, P., Casotto, R., Satish, R.,
698 Mishra, S., Pospisilova, V., Mohr, C., Bell, D. M., Ganguly, D., Verma, V., Rastogi, N., Baltensperger,



699 U., Tripathi, S. N., Prévôt, A. S. H., and Slowik, J. G.: Highly time-resolved chemical speciation and
700 source apportionment of organic aerosol components in Delhi, India, using extractive electrospray
701 ionization mass spectrometry, *Atmos. Chem. Phys.*, 22, 7739-7761, <https://doi.org/10.5194/acp-22-7739-2022>, 2022.

703 Le Breton, M., Hallquist, Å. M., Pathak, R. K., Simpson, D., Wang, Y., Johansson, J., Zheng, J., Yang,
704 Y., Shang, D., Wang, H., Liu, Q., Chan, C., Wang, T., Bannan, T. J., Priestley, M., Percival, C. J.,
705 Shallcross, D. E., Lu, K., Guo, S., Hu, M., and Hallquist, M.: Chlorine oxidation of VOCs at a semi-
706 rural site in Beijing: significant chlorine liberation from ClNO₂ and subsequent gas- and particle-phase
707 Cl-VOC production, *Atmospheric Chemistry and Physics*, 18, 13013-13030,
708 <https://doi.org/10.5194/acp-18-13013-2018>, 2018a.

709 Le Breton, M., Wang, Y., Hallquist, Å. M., Pathak, R. K., Zheng, J., Yang, Y., Shang, D., Glasius, M.,
710 Bannan, T. J., Liu, Q., Chan, C. K., Percival, C. J., Zhu, W., Lou, S., Topping, D., Wang, Y., Yu, J., Lu,
711 K., Guo, S., Hu, M., and Hallquist, M.: Online gas- and particle-phase measurements of organosulfates,
712 organosulfonates and nitrooxy organosulfates in Beijing utilizing a FIGAERO ToF-CIMS,
713 *Atmospheric Chemistry and Physics*, 18, 10355-10371, <https://doi.org/10.5194/acp-18-10355-2018>,
714 2018b.

715 Li, M., Xia, M., Lin, C., Jiang, Y., Sun, W., Wang, Y., Zhang, Y., He, M., and Wang, T.: Mechanistic
716 insights into chloroacetic acid production from atmospheric multiphase volatile organic compound-
717 chlorine chemistry, *Atmos. Chem. Phys.*, 25, 3753-3764, <https://doi.org/10.5194/acp-25-3753-2025>,
718 2025.

719 Lim, Y. B., and Ziemann, P. J.: Chemistry of Secondary Organic Aerosol Formation from OH Radical-
720 Initiated Reactions of Linear, Branched, and Cyclic Alkanes in the Presence of NO_x, *Aerosol Science
721 and Technology*, 43, 604-619, <https://doi.org/10.1080/02786820902802567>, 2009.

722 Liu, X., Qu, H., Huey, L. G., Wang, Y., Sjostedt, S., Zeng, L., Lu, K., Wu, Y., Hu, M., Shao, M., Zhu,
723 T., and Zhang, Y.: High Levels of Daytime Molecular Chlorine and Nitryl Chloride at a Rural Site on
724 the North China Plain, *Environ Sci Technol*, 51, 9588-9595, <https://doi.org/10.1021/acs.est.7b03039>,
725 2017.

726 Ljungström, E., and Hallquist, M.: Nitrate radical formation rates in scandinavia, *Atmospheric
727 Environment*, 30, 2925-2932, [https://doi.org/https://doi.org/10.1016/1352-2310\(96\)00006-4](https://doi.org/https://doi.org/10.1016/1352-2310(96)00006-4), 1996.

728 Lopez-Hilfiker, F. D., Mohr, C., Ehn, M., Rubach, F., Kleist, E., Wildt, J., Mentel, T. F., Lutz, A.,
729 Hallquist, M., Worsnop, D., and Thornton, J. A.: A novel method for online analysis of gas and particle
730 composition: description and evaluation of a Filter Inlet for Gases and AEROsols (FIGAERO),
731 *Atmospheric Measurement Techniques*, 7, 983-1001, <https://doi.org/10.5194/amt-7-983-2014>, 2014.

732 Ma, W., Chen, X., Xia, M., Liu, Y., Wang, Y., Zhang, Y., Zheng, F., Zhan, J., Hua, C., Wang, Z., Wang,
733 W., Fu, P., Kulmala, M., and Liu, Y.: Reactive Chlorine Species Advancing the Atmospheric Oxidation
734 Capacities of Inland Urban Environments, *Environmental Science & Technology*, 57, 14638-14647,
735 <https://doi.org/10.1021/acs.est.3c05169>, 2023.

736 McNamara, S. M., AR, W. R., Wang, S., Thanekar, S., Boone, E. J., Kolesar, K. R., Peterson, P. K.,
737 Simpson, W. R., Fuentes, J. D., Shepson, P. B., and Pratt, K. A.: Springtime Nitrogen Oxide-Influenced
738 Chlorine Chemistry in the Coastal Arctic, *Environ Sci Technol*, 53, 8057-8067,
739 <https://doi.org/10.1021/acs.est.9b01797>, 2019.



740 McNamara, S. M., Kolesar, K. R., Wang, S., Kirpes, R. M., May, N. W., Gunsch, M. J., Cook, R. D.,
741 Fuentes, J. D., Hornbrook, R. S., Apel, E. C., China, S., Laskin, A., and Pratt, K. A.: Observation of
742 Road Salt Aerosol Driving Inland Wintertime Atmospheric Chlorine Chemistry, *ACS Cent Sci*, 6, 684-
743 694, <https://doi.org/10.1021/acscentsci.9b00994>, 2020.

744 Mielke, L. H., Stutz, J., Tsai, C., Hurlock, S. C., Roberts, J. M., Veres, P. R., Froyd, K. D., Hayes, P.
745 L., Cubison, M. J., Jimenez, J. L., Washenfelder, R. A., Young, C. J., Gilman, J. B., Gouw, J. A., Flynn,
746 J. H., Grossberg, N., Lefer, B. L., Liu, J., Weber, R. J., and Osthoff, H. D.: Heterogeneous formation
747 of nitryl chloride and its role as a nocturnal NO_x reservoir species during CalNex - LA 2010, *Journal*
748 *of Geophysical Research: Atmospheres*, 118, 10638-10652, <https://doi.org/10.1002/jgrd.50783>, 2013.

749 Nelson, B. S., Stewart, G. J., Drysdale, W. S., Newland, M. J., Vaughan, A. R., Dunmore, R. E.,
750 Edwards, P. M., Lewis, A. C., Hamilton, J. F., Acton, W. J., Hewitt, C. N., Crilley, L. R., Alam, M. S.,
751 Şahin, Ü. A., Beddows, D. C. S., Bloss, W. J., Slater, E., Whalley, L. K., Heard, D. E., Cash, J. M.,
752 Langford, B., Nemitz, E., Sommariva, R., Cox, S., Shivani, Gadi, R., Gurjar, B. R., Hopkins, J. R.,
753 Rickard, A. R., and Lee, J. D.: In situ ozone production is highly sensitive to volatile organic
754 compounds in Delhi, India, *Atmos. Chem. Phys.*, 21, 13609-13630, <https://doi.org/10.5194/acp-21-13609-2021>, 2021.

755 Noxon, J. F., Norton, R. B., and Marovich, E.: NO₃ in the troposphere, *Geophysical Research Letters*,
756 7, 125-128, <https://doi.org/https://doi.org/10.1029/GL007i002p00125>, 1980.

757 Ogrizek, M., Kroflič, A., and Šala, M.: Critical review on the development of analytical techniques for
758 the elemental analysis of airborne particulate matter, *Trends in Environmental Analytical Chemistry*,
759 33, e00155, <https://doi.org/https://doi.org/10.1016/j.teac.2022.e00155>, 2022.

760 Osthoff, H. D., Roberts, J. M., Ravishankara, A. R., Williams, E. J., Lerner, B. M., Sommariva, R.,
761 Bates, T. S., Coffman, D., Quinn, P. K., Dibb, J. E., Stark, H., Burkholder, J. B., Talukdar, R. K.,
762 Meagher, J., Fehsenfeld, F. C., and Brown, S. S.: High levels of nitryl chloride in the polluted
763 subtropical marine boundary layer, *Nature Geoscience*, 1, 324-328, <https://doi.org/10.1038/ngeo177>,
764 2008.

765 Peng, X., Wang, W., Xia, M., Chen, H., Ravishankara, A. R., Li, Q., Saiz-Lopez, A., Liu, P., Zhang, F.,
766 Zhang, C., Xue, L., Wang, X., George, C., Wang, J., Mu, Y., Chen, J., and Wang, T.: An unexpected
767 large continental source of reactive bromine and chlorine with significant impact on wintertime air
768 quality, *Natl Sci Rev*, 8, nwaa304, <https://doi.org/10.1093/nsr/nwaa304>, 2021.

769 Phillips, G. J., Tang, M. J., Thieser, J., Brickwedde, B., Schuster, G., Bohn, B., Lelieveld, J., and
770 Crowley, J. N.: Significant concentrations of nitryl chloride observed in rural continental Europe
771 associated with the influence of sea salt chloride and anthropogenic emissions, *Geophysical Research*
772 *Letters*, 39, n/a-n/a, <https://doi.org/10.1029/2012gl051912>, 2012.

773 Priestley, M., le Breton, M., Bannan, T. J., Worrall, S. D., Bacak, A., Smedley, A. R. D., Reyes-Villegas,
774 E., Mehra, A., Allan, J., Webb, A. R., Shallcross, D. E., Coe, H., and Percival, C. J.: Observations of
775 organic and inorganic chlorinated compounds and their contribution to chlorine radical concentrations
776 in an urban environment in northern Europe during the wintertime, *Atmospheric Chemistry and*
777 *Physics*, 18, 13481-13493, <https://doi.org/10.5194/acp-18-13481-2018>, 2018.

778 Rai, P., Furger, M., El Haddad, I., Kumar, V., Wang, L., Singh, A., Dixit, K., Bhattu, D., Petit, J.-E.,
779 Ganguly, D., Rastogi, N., Baltensperger, U., Tripathi, S. N., Slowik, J. G., and Prévôt, A. S. H.: Real-
780



781 time measurement and source apportionment of elements in Delhi's atmosphere, *Science of The Total*
782 *Environment*, 742, 140332, <https://doi.org/https://doi.org/10.1016/j.scitotenv.2020.140332>, 2020.

783 Riedel, T. P., Bertram, T. H., Crisp, T. A., Williams, E. J., Lerner, B. M., Vlasenko, A., Li, S. M.,
784 Gilman, J., de Gouw, J., Bon, D. M., Wagner, N. L., Brown, S. S., and Thornton, J. A.: Nitryl chloride
785 and molecular chlorine in the coastal marine boundary layer, *Environ Sci Technol*, 46, 10463-10470,
786 <https://doi.org/10.1021/es204632r>, 2012.

787 Riedel, T. P., Wagner, N. L., Dubé, W. P., Middlebrook, A. M., Young, C. J., Öztürk, F., Bahreini, R.,
788 VandenBoer, T. C., Wolfe, D. E., Williams, E. J., Roberts, J. M., Brown, S. S., and Thornton, J. A.:
789 Chlorine activation within urban or power plant plumes: Vertically resolved ClNO₂ and Cl₂
790 measurements from a tall tower in a polluted continental setting, *Journal of Geophysical Research: Atmospheres*, 118, 8702-8715, <https://doi.org/10.1002/jgrd.50637>, 2013.

791 Sharma, G., Sinha, B., Pallavi, Hakkim, H., Chandra, B. P., Kumar, A., and Sinha, V.: Gridded
792 Emissions of CO, NO_x, SO₂, CO₂, NH₃, HCl, CH₄, PM_{2.5}, PM₁₀, BC, and NMVOC from Open
793 Municipal Waste Burning in India, *Environmental Science & Technology*, 53, 4765-4774,
794 <https://doi.org/10.1021/acs.est.8b07076>, 2019.

795 Simpson, W. R., Brown, S. S., Saiz-Lopez, A., Thornton, J. A., and Glasow, R.: Tropospheric halogen
796 chemistry: sources, cycling, and impacts, *Chem Rev*, 115, 4035-4062,
797 <https://doi.org/10.1021/cr5006638>, 2015.

798 Tham, Y. J., Wang, Z., Li, Q., Yun, H., Wang, W., Wang, X., Xue, L., Lu, K., Ma, N., Bohn, B., Li, X.,
799 Kecorius, S., Größ, J., Shao, M., Wiedensohler, A., Zhang, Y., and Wang, T.: Significant concentrations
800 of nitryl chloride sustained in the morning: investigations of the causes and impacts on ozone
801 production in a polluted region of northern China, *Atmos. Chem. Phys.*, 16, 14959-14977,
802 <https://doi.org/10.5194/acp-16-14959-2016>, 2016a.

803 Tham, Y. J., Wang, Z., Li, Q., Yun, H., Wang, W., Wang, X., Xue, L., Lu, K., Ma, N., Bohn, B., Li, X.,
804 Kecorius, S., Größ, J., Shao, M., Wiedensohler, A., Zhang, Y., and Wang, T.: Significant concentrations
805 of nitryl chloride sustained in the morning: investigations of the causes and impacts on ozone
806 production in a polluted region of northern China, *Atmospheric Chemistry and Physics*, 16, 14959-
807 14977, <https://doi.org/10.5194/acp-16-14959-2016>, 2016b.

808 Tham, Y. J., Wang, Z., Li, Q., Wang, W., Wang, X., Lu, K., Ma, N., Yan, C., Kecorius, S., Wiedensohler,
809 A., Zhang, Y., and Wang, T.: Heterogeneous N₂O₅ uptake coefficient and production yield of ClNO₂
810 in polluted northern China: roles of aerosol water content and chemical composition, *Atmos. Chem.
811 Phys.*, 18, 13155-13171, <https://doi.org/10.5194/acp-18-13155-2018>, 2018.

812 Thornton, J. A., Braban, C. F., and Abbatt, J. P. D.: N₂O₅ hydrolysis on sub-micron organic aerosols:
813 the effect of relative humidity, particle phase, and particle size, *Physical Chemistry Chemical Physics*,
814 5, 4593-4603, <https://doi.org/10.1039/B307498F>, 2003.

815 Thornton, J. A., Kercher, J. P., Riedel, T. P., Wagner, N. L., Cozic, J., Holloway, J. S., Dube, W. P.,
816 Wolfe, G. M., Quinn, P. K., Middlebrook, A. M., Alexander, B., and Brown, S. S.: A large atomic
817 chlorine source inferred from mid-continental reactive nitrogen chemistry, *Nature*, 464, 271-274,
818 <https://doi.org/10.1038/nature08905>, 2010.

819 Trebs, I., Bohn, B., Ammann, C., Rummel, U., Blumthaler, M., Königstedt, R., Meixner, F. X., Fan,
820 S., and Andreae, M. O.: Relationship between the NO₂ photolysis frequency and the solar global



822 irradiance, *Atmos. Meas. Tech.*, 2, 725-739, <https://doi.org/10.5194/amt-2-725-2009>, 2009.

823 Unga, F., Calzolai, G., Chiari, M., Cuccia, E., Colombi, C., Franciosa, M., Dinoi, A., Merico, E.,
824 Pennetta, A., Gómez-Sánchez, N., Mapelli, C., Pareti, S., Perrino, C., Yubero, E., and Contini, D.:
825 Determination of aerosol composition by ED-XRF on Teflon and quartz substrates: potentialities and
826 limits, *Aerosol Research*, 3, 405-415, <https://doi.org/10.5194/ar-3-405-2025>, 2025.

827 Wagner, N. L., Riedel, T. P., Roberts, J. M., Thornton, J. A., Angevine, W. M., Williams, E. J., Lerner,
828 B. M., Vlasenko, A., Li, S. M., Dubé, W. P., Coffman, D. J., Bon, D. M., de Gouw, J. A., Kuster, W.
829 C., Gilman, J. B., and Brown, S. S.: The sea breeze/land breeze circulation in Los Angeles and its
830 influence on nitryl chloride production in this region, *Journal of Geophysical Research: Atmospheres*,
831 117, <https://doi.org/https://doi.org/10.1029/2012JD017810>, 2012.

832 Wang, C., Liggio, J., Wentzell, J. J. B., Jorga, S., Folkerson, A., and Abbatt, J. P. D.: Chloramines as
833 an important photochemical source of chlorine atoms in the urban atmosphere, *Proceedings of the
834 National Academy of Sciences*, 120, e2220889120, <https://doi.org/doi:10.1073/pnas.2220889120>,
835 2023a.

836 Wang, D. S., and Hildebrandt Ruiz, L.: Chlorine-initiated oxidation of n-alkanes under high-NO_x
837 conditions: insights into secondary organic aerosol composition and volatility using a FIGAERO-
838 CIMS, *Atmos. Chem. Phys.*, 18, 15535-15553, <https://doi.org/10.5194/acp-18-15535-2018>, 2018.

839 Wang, D. S., Masoud, C. G., Modi, M., and Hildebrandt Ruiz, L.: Isoprene–Chlorine Oxidation in the
840 Presence of NO_x and Implications for Urban Atmospheric Chemistry, *Environmental Science &
841 Technology*, 56, 9251-9264, <https://doi.org/10.1021/acs.est.1c07048>, 2022.

842 Wang, H., Lu, K., Chen, X., Zhu, Q., Chen, Q., Guo, S., Jiang, M., Li, X., Shang, D., Tan, Z., Wu, Y.,
843 Wu, Z., Zou, Q., Zheng, Y., Zeng, L., Zhu, T., Hu, M., and Zhang, Y.: High N₂O₅ Concentrations
844 Observed in Urban Beijing: Implications of a Large Nitrate Formation Pathway, *Environmental
845 Science & Technology Letters*, 4, 416-420, <https://doi.org/10.1021/acs.estlett.7b00341>, 2017a.

846 Wang, H., Wang, H., Lu, X., Lu, K., Zhang, L., Tham, Y. J., Shi, Z., Aikin, K., Fan, S., Brown, S. S.,
847 and Zhang, Y.: Increased night-time oxidation over China despite widespread decrease across the globe,
848 *Nature Geoscience*, <https://doi.org/10.1038/s41561-022-01122-x>, 2023b.

849 Wang, J., Wang, H., Tham, Y. J., Ming, L., Zheng, Z., Fang, G., Sun, C., Ling, Z., Zhao, J., and Fan,
850 S.: Measurement report: Atmospheric nitrate radical chemistry in the South China Sea influenced by
851 the urban outflow of the Pearl River Delta, *Atmos. Chem. Phys.*, 24, 977-992,
852 <https://doi.org/10.5194/acp-24-977-2024>, 2024.

853 Wang, T., Brown, S. S., Dubé, W. P., Tham, Y. J., Zha, Q., Xue, L., Poon, S., Wang, Z., Blake, D. R.,
854 Tsui, W., and Parrish, D. D.: Observations of nitryl chloride and modeling its source and effect on
855 ozone in the planetary boundary layer of southern China, *Journal of Geophysical Research: Atmospheres*,
856 121, 2457-2475, <https://doi.org/10.1002/2015jd024566>, 2016.

857 Wang, X., Jacob, D. J., Eastham, S. D., Sulprizio, M. P., Zhu, L., Chen, Q., Alexander, B., Sherwen,
858 T., Evans, M. J., Lee, B. H., Haskins, J. D., Lopez-Hilfiker, F. D., Thornton, J. A., Huey, G. L., and
859 Liao, H.: The role of chlorine in global tropospheric chemistry, *Atmospheric Chemistry and Physics*,
860 19, 3981-4003, <https://doi.org/10.5194/acp-19-3981-2019>, 2019.

861 Wang, Z., Wang, W., Tham, Y. J., Li, Q., Wang, H., Wen, L., Wang, X., and Wang, T.: Fast
862 heterogeneous N₂O₅ uptake and ClNO₂ production in power plant and industrial plumes observed in



863 the nocturnal residual layer over the North China Plain, *Atmospheric Chemistry and Physics*, 17, 12361-
864 12378, <https://doi.org/10.5194/acp-17-12361-2017>, 2017b.

865 Wängberg, I., Etzkorn, T., Barnes, I., Platt, U., and Becker, K. H.: Absolute Determination of the
866 Temperature Behavior of the $\text{NO}_2 + \text{NO}_3 + (\text{M}) \leftrightarrow \text{N}_2\text{O}_5 + (\text{M})$ Equilibrium, *The Journal of Physical
867 Chemistry A*, 101, 9694-9698, <https://doi.org/10.1021/jp972203o>, 1997.

868 Xia, M., Peng, X., Wang, W., Yu, C., Sun, P., Li, Y., Liu, Y., Xu, Z., Wang, Z., Xu, Z., Nie, W., Ding,
869 A., and Wang, T.: Significant production of ClNO_2 and possible source of Cl_2 from N_2O_5 uptake at a
870 suburban site in eastern China, *Atmospheric Chemistry and Physics*, 20, 6147-6158,
871 <https://doi.org/10.5194/acp-20-6147-2020>, 2020.

872 Xia, M., Peng, X., Wang, W., Yu, C., Wang, Z., Tham, Y. J., Chen, J., Chen, H., Mu, Y., Zhang, C., Liu,
873 P., Xue, L., Wang, X., Gao, J., Li, H., and Wang, T.: Winter ClNO_2 formation in the region of fresh
874 anthropogenic emissions: seasonal variability and insights into daytime peaks in northern China,
875 *Atmospheric Chemistry and Physics*, 21, 15985-16000, <https://doi.org/10.5194/acp-21-15985-2021>,
876 2021.

877 Xia, M., Jiang, Y., Dai, J., Liu, Y., Yan, C., Kulmala, M., and Wang, T.: Chlorine Activation in Marine
878 Air: Insights From Chemical Budgets of Molecular Chlorine and Hypochlorous Acid, *Journal of
879 Geophysical Research: Atmospheres*, 130, e2024JD042568,
880 <https://doi.org/https://doi.org/10.1029/2024JD042568>, 2025.

881 Xu, T., Takeuchi, M., Rivera-Rios, J. C., and Ng, N. L.: Multigeneration Chemistry in Secondary
882 Organic Aerosol Formation from Nitrate Radical Oxidation of Isoprene, *ACS Earth and Space
883 Chemistry*, 9, 411-423, <https://doi.org/10.1021/acsearthspacechem.4c00417>, 2025.

884 Yan, C., Tham, Y. J., Nie, W., Xia, M., Wang, H., Guo, Y., Ma, W., Zhan, J., Hua, C., Li, Y., Deng, C.,
885 Li, Y., Zheng, F., Chen, X., Li, Q., Zhang, G., Mahajan, A. S., Cuevas, C. A., Huang, D. D., Wang, Z.,
886 Sun, Y., Saiz-Lopez, A., Bianchi, F., Kerminen, V.-M., Worsnop, D. R., Donahue, N. M., Jiang, J., Liu,
887 Y., Ding, A., and Kulmala, M.: Increasing contribution of nighttime nitrogen chemistry to wintertime
888 haze formation in Beijing observed during COVID-19 lockdowns, *Nature Geoscience*,
889 <https://doi.org/10.1038/s41561-023-01285-1>, 2023.

890 Yan, Y., Wang, S., Zhu, J., Guo, Y., Tang, G., Liu, B., An, X., Wang, Y., and Zhou, B.: Vertically
891 increased NO_3 radical in the nocturnal boundary layer, *Science of The Total Environment*, 763, 142969,
892 <https://doi.org/https://doi.org/10.1016/j.scitotenv.2020.142969>, 2021.

893 Yang, X., Wang, Q., Ma, N., Hu, W., Gao, Y., Huang, Z., Zheng, J., Yuan, B., Yang, N., Tao, J., Hong,
894 J., Cheng, Y., and Su, H.: The impact of chlorine chemistry combined with heterogeneous N_2O_5
895 reactions on air quality in China, *Atmos. Chem. Phys.*, 22, 3743-3762, <https://doi.org/10.5194/acp-22-3743-2022>, 2022.

896 Ye, C., Yuan, B., Lin, Y., Wang, Z., Hu, W., Li, T., Chen, W., Wu, C., Wang, C., Huang, S., Qi, J., Wang,
897 B., Wang, C., Song, W., Wang, X., Zheng, E., Krechmer, J. E., Ye, P., Zhang, Z., Wang, X., Worsnop,
898 D. R., and Shao, M.: Chemical characterization of oxygenated organic compounds in the gas phase
899 and particle phase using iodide CIMS with FIGAERO in urban air, *Atmospheric Chemistry and Physics*,
900 21, 8455-8478, <https://doi.org/10.5194/acp-21-8455-2021>, 2021.

901 Young, C. J., Washenfelder, R. A., Roberts, J. M., Mielke, L. H., Osthoff, H. D., Tsai, C., Pikelnaya,
902 O., Stutz, J., Veres, P. R., Cochran, A. K., VandenBoer, T. C., Flynn, J., Grossberg, N., Haman, C. L.,



904 Lefer, B., Stark, H., Graus, M., de Gouw, J., Gilman, J. B., Kuster, W. C., and Brown, S. S.: Vertically
905 Resolved Measurements of Nighttime Radical Reservoirs in Los Angeles and Their Contribution to
906 the Urban Radical Budget, *Environmental Science & Technology*, 46, 10965-10973,
907 <https://doi.org/10.1021/es302206a>, 2012.

908 Zhou, W., Zhao, J., Ouyang, B., Mehra, A., Xu, W., Wang, Y., Bannan, T. J., Worrall, S. D., Priestley,
909 M., Bacak, A., Chen, Q., Xie, C., Wang, Q., Wang, J., Du, W., Zhang, Y., Ge, X., Ye, P., Lee, J. D., Fu,
910 P., Wang, Z., Worsnop, D., Jones, R., Percival, C. J., Coe, H., and Sun, Y.: Production of N₂O₅ and
911 ClNO₂ in summer in urban Beijing, China, *Atmospheric Chemistry and Physics*, 18, 11581-11597,
912 <https://doi.org/10.5194/acp-18-11581-2018>, 2018.

913